

MAY 25 1983

LIBRARIES

EFFICIENCY AND REGIONAL DISTRIBUTION OF HIGH FREQUENCY VENTILATION

by

JOSE GABRIEL VENEGAS T.

B.S., Universidad de los Andes
Bogotá, Colombia (1973)

M.Sc. University of Aston in Birmingham
England, U.K. (1975)

SUBMITTED TO THE HARVARD-MIT DIVISION OF
HEALTH SCIENCES AND TECHNOLOGY IN PARTIAL
FULFILLMENT OF THE REQUIREMENTS FOR THE
DEGREE OF

DOCTOR OF PHILOSOPHY

at the

MASSACHUSETTS INSTITUTE OF TECHNOLOGY

May 1983

**SCHERING-
PLOUGH LIBRARY**

MASSACHUSETTS INSTITUTE
OF TECHNOLOGY

MAY 25 1983

LIBRARIES

Signature of Author

[Handwritten signature]

Harvard-MIT Division of Health Sciences and Technology
May 27, 1983

Certified by

[Handwritten initials]

Prof. Ascher H. Shapiro
Thesis Supervisor

Certified by

Dr Charles A. Hales
Thesis Supervisor

Accepted by

[Handwritten initials]

Prof. Ernest G. Cravalho
Chairman, Division Committee on Graduate Theses

EFFICIENCY AND REGIONAL DISTRIBUTION OF HIGH FREQUENCY VENTILATION

by

JOSE GABRIEL VENEGAS T.

Submitted to the Harvard-MIT Division of Health Sciences and Technology on May 27, 1983 in partial fulfillment of the requirements for the degree of DOCTOR OF PHILOSOPHY.

Abstract

The overall efficacy and regional distribution of ventilation during *High Frequency Ventilation (HFV)* in dogs when tidal volume (V_t) was similar or less than anatomic dead space were examined. Efficacy and distribution of ventilation were assessed by imaging, with a positron camera, a washout of the positron emitting isotope (^{13}N) from the lungs of anesthetized, paralyzed, supine animals. *HFV* was delivered with a High Frequency Ventilator, developed by us, that generated tidal volumes (V_t) (20cc to 150cc), independent of the animal's lung impedance, at frequencies (f) from 1 to 25 Hz, with a square flow rate wave form and a variable exhalation to inhalation ratio (E:I) (1:1 to 1:4). From our results we conclude that the Functional Residual Capacity (*FRC*) volume is a major normalizing parameter in the sense that (V_t/FRC), rather than V_t alone, correlates the results from different animals. A relationship was established to predict the eucapnic settings of the respirator given the dog lung volume and weight. The overall specific alveolar ventilation (*SPVENT*) was found to follow closely the relation: $\text{SPVENT} \approx 1.9(V_t/\text{FRC})^{2.1} \times f$. A pattern of preferential basal ventilation was found, that became less significant with the combinations of smaller V_t and higher f . However, at a constant ($V_t \times f$) product, an increase of V_t produced a significant overall increase in alveolar ventilation. A set of similar studies comparing the distribution of ventilation during localized partial airway obstruction showed that the ventilation distribution is more adversely affected during *HFV* than during conventional ventilation. This finding reveals the possibility of using the technique, developed in this thesis work, as a non-invasive method of detecting, at early stages, obstructions of the large bronchi.

Thesis Supervisors: Prof. Ascher H. Shapiro

Title: Institute Professor

Dr Charles A. Hales

Title: Associate Professor of Medicine Harvard Medical School

Thesis Committee: A. H. Shapiro PhD.
C. A. Hales MD.
R. D. Kamm PhD.
J. Custer MD.
B. Hoop PhD.
R. H. Ingram Jr. MD.
E. G. Cravalho PhD.

Table of Contents

Abstract	2
Table of Contents	3
ACKNOWLEDGEMENTS	6
NOMENCLATURE	8
PROLOGUE	10
1. INTRODUCTION	11
1.1 <i>Objectives</i>	12
2. APPARATUS	14
2.1 <i>The High Frequency Ventilator</i>	14
2.2 <i>The Experimental Apparatus</i>	16
3. METHODS	19
3.1 <i>Experimental procedure</i>	19
3.1.1 Normal Animals	20
3.1.1.1 Protocol #1	20
3.1.1.2 Protocol #2	21
3.1.2 Protocol #3, Partially Obstructed Airway	22
3.2 <i>Lung Volume Measurement</i>	22
4. DATA ANALYSIS	24
4.1 <i>Normal Dogs</i>	24
4.1.1 Total Lung Washout	24
4.1.2 Specific Alveolar Ventilation	24
4.1.3 <i>MTT</i> Functional Images	27
4.1.4 Specific Ventilation Histograms	28
4.1.4.1 Error Estimation	30
4.1.5 Regional Specific Ventilation	32
4.1.6 Geometrical Considerations	32
4.2 <i>Partially Occluded Airway</i>	35
5. RESULTS	36
5.1 <i>Whole-lung Ventilation</i>	36
5.1.1 Specific alveolar ventilation	36
5.1.1.1 Protocol#2	37
5.1.1.2 Protocol #1	41
5.1.2 Specific Ventilation and CO ₂ transport.	47
5.1.3 The <i>HFV</i> Equation.	50
5.1.4 Efficiency of <i>HFV</i> and <i>CV</i>	50
5.2 <i>Regional Distribution of Ventilation</i>	53

5.2.1 MTT Functional Images	53
5.2.2 Quantitative analysis	56
5.2.2.1 Spread of Specific Ventilation Histograms	58
5.2.3 Regions of interest	61
5.2.3.1 Right Lung vs Left Lung Specific Ventilation	62
5.2.3.2 Basal vs Apical Ventilation	65
5.3 <i>Summary of results in normal dogs</i>	67
5.4 <i>Partially Occluded Airway</i>	68
6. DISCUSSION	71
6.1 <i>Total Lung Ventilation</i>	71
6.2 <i>Distribution of ventilation</i>	76
6.2.1 Direct Alveolar Ventilation	77
6.2.2 Geometry of the Bifurcating Tree	78
6.2.3 Distribution of Dynamic Impedances	80
6.3 <i>Gas Transport Distribution</i>	84
6.3.1 Interregional Mixing	84
6.4 <i>Previous Work</i>	84
6.5 <i>Cross-sectional Area</i>	87
7. CONCLUSIONS	88
Appendix A. PULMONARY VENTILATION	90
A.1 Physiology of Normal Respiration	90
A.2 Artificial Ventilation	91
A.3 Distribution of Ventilation	92
A.4 Measurement of Distribution of Ventilation	93
Appendix B. MECHANISM OF HFV	95
B.1 Augmented Dispersion	95
B.2 Streaming due to Asymmetric Velocity Profiles	96
B.3 Pendelluft	96
B.4 Direct Alveolar Ventilation.	97
Appendix C. THE HIGH FREQUENCY VENTILATOR	99
C.1 Description	99
C.2 Calibration Tests	101
C.3 Characteristics and Advantages	103
Appendix D. MEASUREMENT ACCURACY	104
D.1 The Positron Camera	104
D.2 Mean Transit Time Image	106
D.3 MTT Correction	108
D.4 Relative Error of Volume Measurement	110
D.5 Histogram Generation	110
Appendix E. NON-INVASIVE METHOD TO DIAGNOSE AIRWAY OBSTRUCTION	113
List of Figures	116

List of Tables

ACKNOWLEDGEMENTS

I want to express my gratitude and admiration to Professor Asher Shapiro. Through his advice and assistance I have gained a new perspective of engineering research. Through his patient guidance, I have learned to study in a more structured manner the exciting puzzles of science. I am equally indebted to Doctor Charles Hales. He enriched my knowledge of respiratory physiology and gave me deep insights into the medical implications of this thesis. Furthermore, he offered me the invaluable opportunity of working at the Massachusetts General Hospital where I found an intellectually stimulating environment, a constructive and helpful working team, and a warm and friendly camaraderie. From the Pulmonary Unit of MGH I want to thank its Chief, Doctor Homayaoun Kazemi for his support and Doctor Joseph Custer, Doctor Bernard Hoop and Paul Pappas for their enthusiasm and direct involvement in the experiments. Many thanks also to William Bucelewicz, Lawrence Beagla, Christopher Buckley, Steven Weise, John Correia and Charles Burnham for their cooperation.

I am very grateful to Professor Roger Kamm for his constructive criticisms and valuable help, and to Professor Ernest Cravalho and Doctor Roland Ingram Jr. for their involvement in my thesis committee and their useful comments.

In this thesis, as in all work coming out of the MIT Fluid Mechanics Lab, the help and assistance of Dick Fenner in putting together experimental apparatus was of crucial importance. The friendly cooperation of Will Gilbert in the data crunching and of Martha Gray, Maria Clemencia Venegas, and Lesley Sharp in the final editing of the manuscript is deeply appreciated.

Finally, I am indebted to my uncle Carlos A Torres, and to the Organization of American States, the Harvard-MIT Division of Health Science and Technology and the grant

No HL 26566 from the National Institute of Health for providing financial support.

NOMENCLATURE

- A = area (cm^2)
 a = bronchial diameter (cm)
 BW = body weight (Kg)
 $c(t)$ = count rate (counts/sec)
 $C_{tr}(x)$ = volume concentration of tracer gas
 C_A = apical compliance
 C_B = basal compliance
 CO_2 = carbon dioxide
 CV = conventional ventilation
 $E:I$ = Expiration/Inspiration time-ratio
 ERR = standard deviation of "error histogram"
 f = frequency (Hz.)
 FA_{CO_2} = alveolar fractional concentration of CO_2
 FRC = Functional Residual Capacity (cc.)
 fd = fractional volume density
 HFV = High Frequency Ventilation
 h = fractional volume of hyper-ventilated region
 MTT = mean transit time (sec.)
 N = number of counts
 ^{13}NN = Nitrogen 13 labeled Nitrogen
 O_2 = Oxygen
 L = Inductance
 $p(t)$ = pressure
 Pa_{CO_2} = Arterial CO_2 Partial Pressure (mm. Hg)
 Pa_{O_2} = Arterial O_2 Partial Pressure (mm. Hg)
 Q = flow rate through HFV device (cc/sec)
 Rey = Reynolds Number
 R = Resistance to flow (cm H_2O sec /cc)
 $SIGMA$ = Corrected spread of regional *SPVENT* histogram.
 $SPVENT$ = Specific ventilation (sec^{-1})
 $SPVENT_f$ = *SPVENT* of fast region (sec^{-1})
 $SPVENT_s$ = *SPVENT* of slow region (sec^{-1})
 $STDEV$ = Standard Deviation of *SPVENT* histogram
 t = time (sec)
 \dot{V}_{alv} = alveolar ventilation (cc/sec)
 \dot{V}_{in} = flow rate through rotary valve (cc/sec)
 \dot{V}_{out} = flow rate through expiratory tube (cc/sec)
 $VENT$ = \dot{V}_{alv} per Kg. of body weight (cc/sec.Kg)
 $VENT_n$ = normocapnic *VENT* (cc/sec.Kg)
 V_i = volume of compartment i (cc.)
 V_t = tidal volume (cc.)
 V_{tot} = total lung volume (cc.)
 α = Womersley parameter = $a \sqrt{2\pi f / \nu}$
 Δ = concentration difference

η = efficiency
 ν = kinematic viscosity (cm²/sec)
 τ = time constant (sec)

PROLOGUE

The body of this thesis is written in the form of a scientific report directed to readers familiar with the subject of respiratory physiology. For completeness more detailed information is added at the end, in the form of several appendices.

Chapter 1

INTRODUCTION

High Frequency Ventilation (HFV) is a novel modality of artificial ventilatory support that uses small tidal volumes at frequencies much greater than the normal. Because of the small volumes, the mean alveolar and bronchial pressures can be smaller than the ones used in conventional ventilation. This fact makes *HFV* ideal for the management of cases where conventional ventilation (*CV*) requires excessive intrapulmonary pressures to operate as in pulmonary edema (Schuster et al., 1981), or cases of bronchial air-leaks as in bronchopleural fistula. A different application of *HFV*, used in conjunction with *CV* for the management of chronic obstructive lung disease, has also been proposed (Venegas, 1975) and tested in patients to decrease air trapping during exhalation. (Venegas and Venegas, 1977, 1979).

Since the tidal volumes used in HFV are equal to or smaller than the anatomical dead space volume, the predictions from classical models for physiologic gas exchange are no longer valid, and new theories and models for gas exchange mechanisms have been recently proposed (Slutsky et al., 1980, Fredberg, 1980, Haselton and Scherer, 1980). (see Appendix B)

Some of these models predict the individual effect of the tidal volume (V_t), frequency (f) and lung volume on the transport of CO_2 . The transport of CO_2 has been experimentally studied during HFV, in dogs (Slutsky et al., 1981) and in humans (Rossing, 1981), by measuring the amount of CO_2 eliminated during the first seconds of HFV. Although the experimental data seemed to follow in general the predictions of the models, there is not yet an empirical or theoretical expression that can reliably predict quantitatively the settings of V_t and f that are needed for eucapnic ventilation in dogs or human patients.

It is well-established that matching between regional ventilation and perfusion is of

fundamental importance in determining the overall efficacy of gas exchange in the lungs (West, 1977). However, all the theories and models just mentioned assume that the alveolar compartment is a single well-mixed chamber and only a few attempts have been made to validate that assumption. The effects of HFV on regional pulmonary ^{133}Xe clearance after equilibration, using sinusoidal oscillations, have been studied for one value of tidal volume at two oscillatory frequencies (Schmid et al., 1981). At the lowest f a small difference between the ventilation of the apical and the basal regions was found. At the higher values of f (with the same V_t), this difference became even smaller. The distribution of ventilation-perfusion ratios during HFV has also been studied recently (Robertson et al., 1982, McEvoy et al., 1982) using the multiple inert gas elimination method. In contrast to Schmid's work, these studies showed gross ventilation-perfusion inequalities, but the results were affected by a gas transport artifact in the more soluble gases. The conflicting results from the above-mentioned reports will be discussed individually in section 6.4.

To the present time, no attempt has been made to study the independent effects of tidal volume and frequency on the distribution of ventilation during HFV.

1.1 Objectives

The main objective of this thesis research is to study experimentally the effects of tidal volume and frequency on both the alveolar ventilation of the whole lung and the regional distribution of specific ventilation during HFV.

A subsidiary objective, required to accomplish the foregoing goal, is the design, construction and testing of a high frequency ventilator with several novel features and advantages over most devices described in the literature.

A further objective of this work is to provide the groundwork for the development of a new technique for early non-invasive diagnosis of large airway obstructions using a technique

similar to the one used in this work. This application is further discussed in Appendix E.

Chapter 2

APPARATUS

2.1 *The High Frequency Ventilator*

This section provides a brief description of the *HFV* apparatus. In Appendix C a more thorough description is provided together with a summary of the calibration tests performed. Figure 2-1 shows a schematic of the flow system.

It consists of a regulated flow source which is chopped by a rotary valve and then introduced to the animal through a 10 mm. ID endotracheal tube. A constant pressure-regulated vacuum supply exhausts the exhalation gases from the animal, at a steady rate, through a high impedance 2 mm. ID, 30 cm long tube as shown in Fig. 2-2.

The apparatus produces a square flow waveform for frequencies from 1 to 20 Hz and can deliver tidal volumes of up to 150 cc. Samples of the delivered tidal volume waveform are shown in Figure 2-3.

Advantages of the design are :

- Delivery of a predictable tidal volume independent of the animal's lung impedance.
- A controlled mean airway pressure, and Functional Residual Capacity (FRC).
- Variability of the exhalation to inhalation time ratio (E:I).
- Full tidal volume consisting of 100 % fresh gas.

HFV SYSTEM

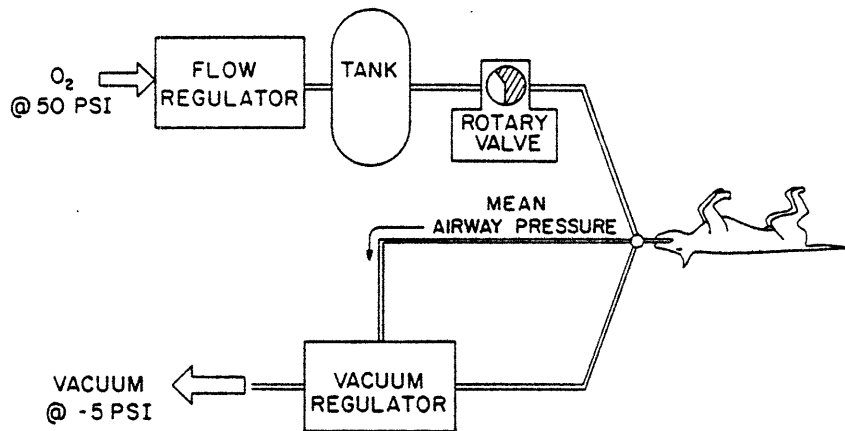


Figure 2-1:
Schematic of the flow system of the HFV ventilator.
For detailed description see appendix C

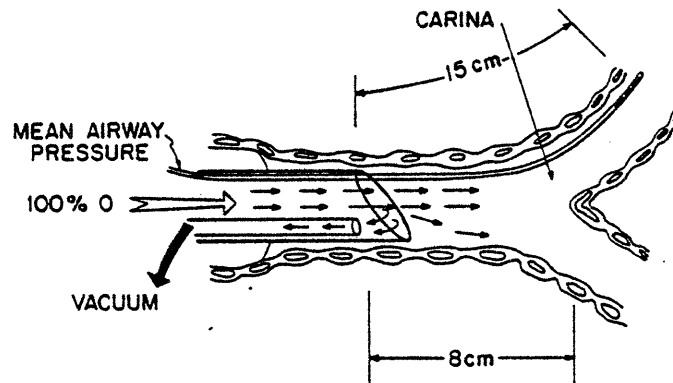


Figure 2-2:
Showing the configuration of inspiratory and expiratory lines and the location of the mean airway pressure catheter.

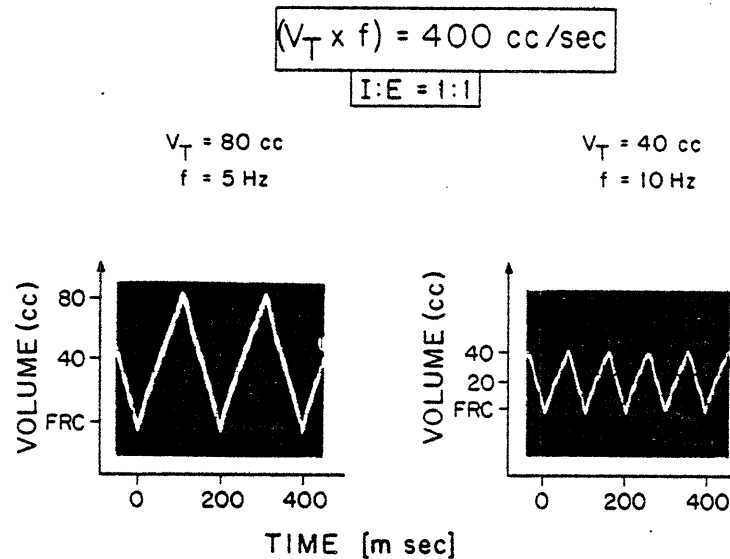


Figure 2-3:

Graph showing the delivered volume waveform vs time as measured from the pressure oscillations induced by the *HFV* device in a calibration tank. The two charts are for for two different settings of V_t and f but the same $(V_t \times f)$ product and the same $E:I=1$.

2.2 The Experimental Apparatus

The experimental apparatus used to study the total and regional distribution of ventilation in dogs is shown schematically in Figure 2-4.

The apparatus consisted of a conventional ventilator plus a rebreathing circuit connected to the animal in parallel with the *HFV* system. Depending on the setting of the two solenoid valves, the *HFV* system ventilated either a calibration tank, simulating a dummy lung, or the animal.

A cyclotron generated positron-emitting radio-isotope Nitrogen-13 labeled Nitrogen gas (^{13}NN). This tracer was introduced into the rebreathing circuit while the animal was

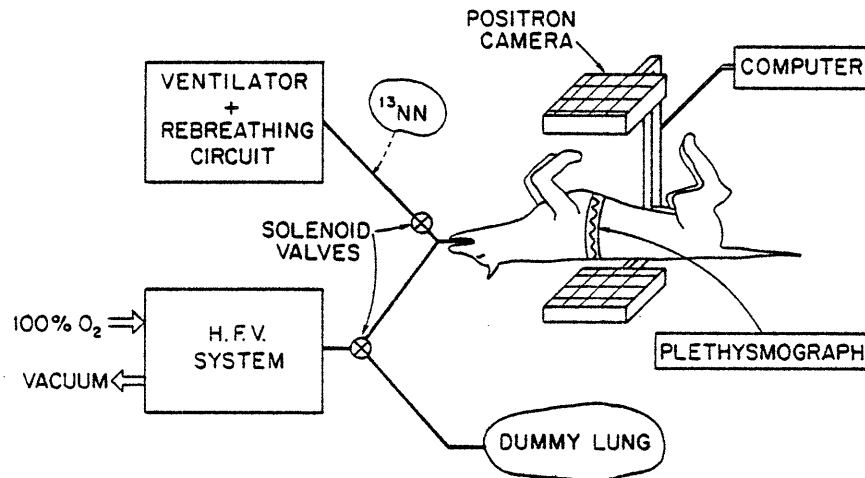


Figure 2-4:
Schematic showing the experimental apparatus set-up to study the regional distribution of ventilation during *HFV*.

ventilated at normocapnea with conventional ventilation (CV) until the ^{13}NN was equilibrated through the system.

A positron camera was used to image the lungs of the animals during a washout maneuver, as described in detail below. The characteristics of the positron camera are presented in Appendix D.1.

Due to the low solubility of nitrogen in blood and tissue, the distribution of the ^{13}NN in the lungs was confined largely to the air volume of the lungs. Other gases used in respiratory imaging, such as Xenon-133, are much more soluble in blood and tissues and thus create a large background noise that has to be corrected during the final analysis. Another advantage of using ^{13}NN was its short half-life of only 9.96 minutes. This allowed us to perform several studies on the same animal without having to wait for long periods of time between runs.

Mean lung volume was monitored using an impedance plethysmograph by RespiTrace, fixed around the chest to the animal

Mean airway pressure and arterial femoral pressure were monitored with pressure transducers and were recorded together with the impedance plethysmographic signal on a chart recorder.

Chapter 3

METHODS

3.1 *Experimental procedure*

A methodology similar to one previously reported (Secker-Walker et al., 1973, Alpert et al., 1976) was used to measure the regional distribution of alveolar ventilation.

Dogs weighing from 16 to 30 kg were anesthetised with 30 mg/kg of pentobarbital and then paralyzed with .05 mg/kg of pancuronium bromide. Respiration was supported by a Harvard animal ventilator set at conventional ventilation (*CV*) with a tidal volume of 15 cc/Kg and a frequency of 15 breaths per minute. Polyethylene catheters were placed in the femoral artery and vein for injection or sampling sites and for monitoring arterial pressure.

A 5 cc. syringe introduced ^{13}NN into the rebreathing system and the animal was ventilated at normocapnea for five minutes. Preliminary tests proved that by this time the total amount of activity in the animal had reached a steady value, thus ensuring that the tracer was homogeneously distributed within the lung.

After the equilibration maneuver, the Harvard respirator was turned off during exhalation and the animal was allowed to exhale to its Functional Residual Capacity (*FRC*).

The positron camera then collected a 10 seconds image of the equilibrated lung volume at *FRC*. The animals were immediately switched to *HFV* with 100% O_2 and 14 sequential images were collected throughout the washout of ^{13}NN from the lung. The collection periods for each of the images were: 5 seconds for the first four images, 15 seconds for the following eight images and 30 seconds for the last two. The inter-frame time was only 0.1sec. and thus the collection of the images, for practical purposes, can be considered continuous. Each

image consisted of a 64-by-64 array of numbers, each corresponding to the number of decay events (*counts*) detected along the vertical line between each pair of opposite detectors from the positron camera (see Appendix D.1). The computer automatically corrected for a change of count rate due to radioactive decay of the ^{13}NN .

The tidal volumes used in *HFV* were measured from the pressure signal produced in a calibrated tank. The latter served as a dummy lung in the period before each washout during which the animal was ventilated with the Harvard ventilator.

It was critically important to maintain the lung volume at a constant *FRC* during the experimental maneuver, since the calculation of the true washout rate is dependent not only on the ventilatory parameters but also on the rate-of-change of lung volume. For this reason, the vacuum regulator was added to the circuit in order to prevent transients in the animal's lung volume at the time of change from *CV* to *HFV*.

Arterial blood samples were obtained from the animal prior to the onset of *HFV* and just after the last image was collected (About 4 minutes after switching to *HFV*). Values of arterial PO_2 , PCO_2 and pH were measured with a blood gas analyzer manufactured by Instrumentation Laboratories set at 37°C .

3.1.1 Normal Animals

In general, the experiments consisted of a series of equilibrations and washout runs for each animal. Before each run the settings of the high frequency ventilator were adjusted to new values of tidal volume and frequency. These parameters were varied systematically according to one of the following two protocols used.

3.1.1.1 Protocol #1

Protocol #1 was motivated by the results reported recently (Slutsky et al., 1981) showing that CO_2 elimination, during *HFV*, is primarily dependent on the product of V_t and

f and is at most weakly dependent of the *FRC* lung volume. Given this, we reasoned that it would be very useful to elucidate which combination of V_t and f would produce the most homogeneous ventilation. In order to minimize the length of the studies, we tried to study *HFV* only at the 'eucapnic' oscillatory flow rates ($V_t \times f$).

We sought the eucapnic value of ($V_t \times f$), in eight of the animals. In these explorations, ($V_t \times f$) and E:I were fixed to particular constant value and three or four runs were performed varying the tidal volume (V_t) and with it the corresponding frequency (f). The oscillatory flow rate ($V_t \times f$) and or the I:E were then changed to different values and a new set of four runs was performed. V_t varied typically from 20 cc. to 140 cc. In this protocol 2/3 of the runs were made using an E:I=1 and the rest were made with either E:I=2 or E:I=4.

Our results did not agree with the aforementioned CO_2 elimination findings (Slutsky et al., 1981) in that the eucapnic ventilation could be obtained in the same dog with different values of ($V_t \times f$),¹ the protocol was modified to a more focused experiment in which we studied only the E:I=1 as explained in the following paragraph.

3.1.1.2 Protocol #2

Using six animals, V_t was fixed either to 40 cc or 80 cc. and the product ($V_t \times f$) was changed systematically from 150 cc/sec to 450 cc/sec in intervals of 50 cc/sec. The I:E ratio was kept constant and equal to unity.

The lung volume at Functional Residual Capacity (*FRC*) was measured with a method that will be described in section 3.2.

¹More recent experiments from the same group using an improved ventilator, have also found differences with the earlier reports (Gavriely and Solway, 1983). Some possible reasons for the disagreement are discussed in chapter 8

3.1.2 Protocol #3, Partially Obstructed Airway

A set of three animals was used to compare the distribution of ventilation obtained with normal ventilation versus the one obtained with *HFV* under condition of partial airway obstruction.

A SWAN'S GANZ catheter was introduced bronchoscopically and positioned so that, when its balloon was inflated, it would partially obstruct a lower lobe bronchus from one of the lungs.

Both the *HFV* system and the conventional ventilator were set so that the animal would be ventilated at normocapnea with either system.

An equilibration maneuver with ^{13}NN was first conducted in each test with the balloon deflated. Washout runs, as controls, were then performed with the balloon deflated. Subsequently, washout runs were conducted, for both *HFV* and CV, with the balloon inflated with 1.5 cc. of air.

3.2 Lung Volume Measurement

At the beginning or at the end of each experiment under protocol #2, the lung volume at *FRC* of each animal was measured with a novel technique developed by us. The method can be described as follows:

After equilibration with ^{13}NN a 5-second image collection at *FRC* was followed by an inflation of the lungs with an additional 500 cc. of gas from the rebreathing circuit, having the same composition as that used in the equilibration. After a second collection of 5 seconds, the animal was allowed to return to *FRC* by passive exhalation. The procedure was repeated three times. Applying a mass balance to the ^{13}NN , the lung volume at *FRC* may be calculated from the formula:

$$\frac{N_1}{FRC} = \frac{N_2}{(FRC + 500)} \quad (3.1)$$

Where

N_1 = total number of counts at *FRC*

and

N_2 = total number of counts at *FRC* + 500 cc.

The average of the three measurements was used in later calculations.

Chapter 4

DATA ANALYSIS

This chapter gives a general description of the numerical manipulation of the data collected with the positron camera. The first section covers the data obtained from the normal dogs and the second section the data from the experimental bronchial obstruction.

4.1 *Normal Dogs*

4.1.1 Total Lung Washout

The sum of all the counts in the lung field in each image, normalized by the corresponding collection time and the initial count rate, is plotted versus time using semi-log scales in Figure 4-1 for two typical runs. Visual images of the concentration of ^{13}NN collected at about 40 % of the initial concentration are also shown (darker in the gray scale means less concentration of ^{13}NN). Notice that the lower washout curve in the graph is not a straight line and, thus, it is not appropriate to characterize it by its slope. For this reason we chose to use the concept of 'Specific Alveolar Ventilation' (*SPVENT*) which will be presented in the next paragraphs.

4.1.2 Specific Alveolar Ventilation

Analysis of the washout data such as that of Figure 4-1 has usually been limited to single- or multi-compartment models of washout. Several investigators, however have shown that the single parameter "mean transit time" (*MTT*) can be used to characterize regional distribution of ventilation while making no assumptions regarding the number of compartments or their inter-communications. (Secker-Walker et al., 1973, Zierler, 1965, Alpert

In other words *MTT*, for the whole lung or for any individual region, can be defined as the area under a fractional concentration washout curve such as those of Figure 4-1. It represents the mean residence time of a molecule of ^{13}NN in that particular area of the lungs during a washout.

It can be shown that the *MTT* for a mono-exponential washout curve is identical to its time constant (τ) by evaluating the integral in equation (4.2) for $c(t)=c(0) e^{-t/\tau}$. Similarly, the *MTT* for a multi-compartmental mode can be calculated by solving equation (4.2) for:

$$c(t) = \frac{\sum V_j e^{(-t/\tau_j)}}{V_{\text{tot}}} \quad (4.3)$$

where

τ_j = the time constant for compartment (j)

V_{tot} = the total volume of the region

and

V_j = the volume of the compartment (j)

thus yielding the expression:

$$MTT = \sum_j \frac{V_j}{V_{\text{tot}}} \tau_j \quad (4.4)$$

that can be identified as the volume-weighted average of the individual compartment time constants (τ_j).

Since the washout was performed during a finite time, the resulting *MTT* measurement has to be corrected by estimating contribution to *MTT* corresponding in the integral of equation (4.2) to the time between the end of collection and infinity. Note that the $(c(t)/c(0)) \rightarrow 0$ as $t \rightarrow \infty$, and the nature of the attenuation of $(c(t)/c(0))$ with t is such that the integral is expected to be rapidly convergent. The details of the correction procedure are described in Appendix D.3.

The specific ventilation (*SPVENT*) is defined as the inverse of the *MTT*. So, *SPVENT* has units of (sec^{-1}) and represents the alveolar ventilation (e.g., cc/sec) per unit of lung volume (e.g., cc). The concepts of *MTT* and its converse *SPVENT* can be applied either regionally or to the lung as a whole. Moreover, they are especially suitable for washout rate measurements in the lung because the results automatically normalize the rate of tracer clearance to the lung volume.

4.1.3 *MTT* Functional Images

In order to create an image proportional to the regional *MTT*, one has to use equation (4.1) to calculate the individual MTT_i for each pixel (i).

Because the relative small number of counts per pixel produces a relative large statistical uncertainty in the expression, several operations were performed on the data in order to improve the signal-to-noise ratio (see Appendix D.1). These are summarized below.

Instead of using the equilibration image collected in each run, a *mean equilibration image* was created by doing the sum of all the equilibration images collected from the same dog during the experiment. In this way, the expected relative error was decreased proportionally to the square root of the number of images. For this to be correct, it is necessary (and it was assumed) that the lung volume (total and regional) remains the same from run to run. This is not unreasonable as the dog was paralyzed and strapped in position so that it could not move. A further justification for this assumption comes from the calculation of the variance of the measured fractional volumes in four regions (Right Apex, Right Base, Left Apex and Left Base). It was found that the measured variance was not significantly different from the expected variance of the same variables calculated from the statistical properties of the radioactive decay. In other words, the variations during successive runs of the measured fractional volumes at FRC could be explained entirely by the random radioactive decay of the ^{13}NN . Thus the run-to-run changes in the equilibrated gas distributions could be

considered insignificant (see Appendix D.4).

To improve further the signal-to-noise ratio, a smoothing function was applied to the equilibration image and to the washout image before their ratio was calculated. The nature of the smoothing function and its statistical implications are presented in Appendix D.1. For the present purpose it is sufficient to say that by smoothing an image, spatial resolution is sacrificed to favor an improved statistical certainty.

The resulting array of regional values proportional to MTT resulting from the mathematical operations described above was used to generate a gray-scale visual image in which the light areas correspond to the regions with longer MTT and the dark areas to the regions with the shorter MTT . Typical MTT images of this type are presented in Figure 4-2. The bar on the right of the pictures represents the exponential gray scale used. These images are normalized so that the pixel of maximum MTT appears with the maximum degree of whiteness; thus the pictures show relative MTT values. Both images were obtained during washout runs with the same $(Vt \times f) = 300$ [cc./sec] but with different combinations of Vt and f . For the run of the left side the HFV ventilator was set at $Vt=100$ cc. and $f=3$ Hz, and for the one of the right, at $Vt=25$ cc. and $f=12$ Hz.

4.1.4 Specific Ventilation Histograms

From the MTT images, histograms showing the distribution of the normalized regional-specific ventilation vs fraction of lung volume were generated. Appendix D.5 describes the methods used to generate the histograms.

The bottom of Figure 4-2 presents the histograms corresponding to the images at the top. The horizontal scale is the fractional variation of the regional $SPVENT$ from the mean $SPVENT$ (\overline{SPVENT}). The vertical scale is a fractional volume density (fvd) function analogous to a probability density function. The latter is normalized such that the total area under the curve is unity. The area (A) under the curve between the points X_1 and X_2 in



The Libraries
Massachusetts Institute of Technology
Cambridge, Massachusetts 02139

Institute Archives and Special Collections
Room 14N-118
(617) 253-5688

There is no text material missing here.
Pages have been incorrectly numbered.

the histogram at the left, represents the fraction of lung volume having a *SPVENT* which lies between the values X_1 and X_2 .

If the distribution of regional *SPVENT* were perfectly homogeneous, the histogram would be a 'delta' function (with area = 1) located at zero on the horizontal scale, because all the lung volume would be ventilated with the same *SPVENT*. However, since different regions of the lung are ventilated at different rates, the spread of the histogram represents the degree of departure of the regional *SPVENT* from the whole-lung \overline{SPVENT} . This effect can be clearly seen when comparing the two histograms and the respective *MTT* images presented in Figure 4-2. The run on the left produced a less homogeneous distribution of ventilation than the run on the right. This fact is made evident by the great difference between the basal and apical values of *MTT* as shown in the *MTT* image, as well as by the greater spread and the bimodal distribution in the histogram.

4.1.4.1 Error Estimation

Because of the statistics of the measuring process, the standard deviation of the *SPVENT* histogram (*STDEV*) is due not only to the real spread of the parameter but also to the spread caused by the statistics of the measurement. In order to estimate the magnitude of the spread caused by the measurement, an equivalent "error image" for each run was created by dividing the equilibration image obtained for that run by the "mean equilibration image" described in section 4.1.3. The resulting *error images* were processed with the same algorithms as the *MTT* image. An error histogram representing the spread of the data caused by the measuring method was then determined, scaled to the square root of the ratio of the total number of counts between the *error image* to that in the *MTT* image. The standard deviation of the scaled error histogram (*ERR*) was then calculated. Figure 4-3 presents, for the purpose of illustration, an example of the accumulative or integrated fractional volume density functions of the regional *SPVENT* and the scaled error histograms. The vertical axis

represents the fraction of lung volume which has a *SPVENT* greater or equal to the corresponding value of the horizontal axis. Notice the steep rise of the error function representing a narrow spread of the equivalent histogram.

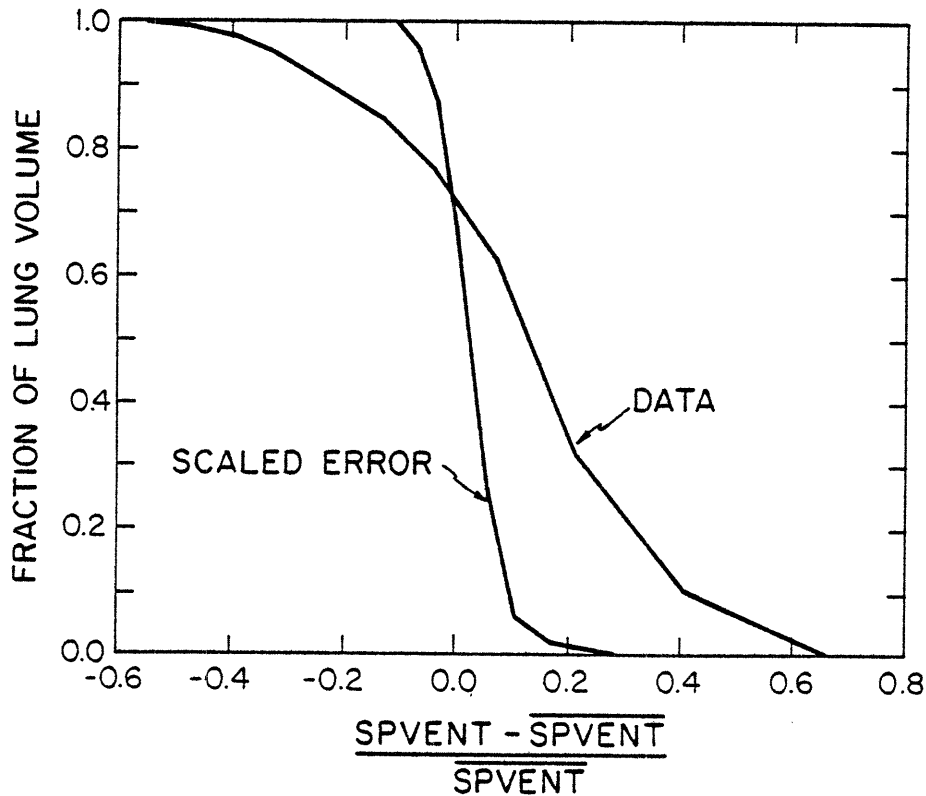


Figure 4-3:
Graph showing a typical curve of fraction of lung volume vs normalized regional *SPVENT* and its corresponding measurement error estimate. (for explanation see text)

Since the "measurement error" is responsible for part of the spread of the *SPVENT* histogram, the spread due to non-homogeneous ventilation alone (*SIGMA*), as opposed to adventitious statistical variations, can be estimated, from basic statistics, as the square root of the difference between the square of the standard deviation of the *SPVENT* histogram and square of the standard deviation of the scaled error histogram

$$SIGMA = \sqrt{STDEV^2 - ERR^2}$$

Although we were comparing *HFV* at different settings, all having similar errors, the use of *SIGMA* instead of *STDEV* eliminates from the data fluctuations in the error from run

to run due to changes in the equilibrated level of radioactivity or decreased number of counts due to faster washout rates.

4.1.5 Regional Specific Ventilation

"Regions of interest" were defined by dividing the lung into four zones by means of a vertical line through the mediastinum and a horizontal line approximately half-way between the apex and the base of the lungs. The values of the specific ventilation in each run for these four regions, as well as for the sum of the right and left apical regions (APEX), the sum of the right and left basal regions (BASE), the sum of the right lung (RIGHT), and the sum of the left lung (LEFT), were calculated from the unsmoothed raw data and corrected with the same method described for the total lung.

4.1.6 Geometrical Considerations

One has to be very cautious when drawing conclusions from the shape of the histograms of *SPVENT* because these are made from a two-dimensional image of the lungs which may have large variations in the third dimension.

In the example illustrated in Figure 4-4, a cube of dimensions $3 \times 3 \times 3$ has a region, in the center, with a *SPVENT* four times greater than that of similar-sized regions in the rest of the cube. The histogram which would be generated from a 3-D image (if it could be determined) has one peak of height= $26/27$ units of volume located at -0.11, and a second peak of height= $1/27$ located at 2.7. In contrast, the histogram generated from the 2-D projection, has the major peak of height= $24/27$ units and the second peak of height= $3/27$ located at 1. In other words, creating a histogram from a 2-D projection image moved the two peaks closer together and increased the apparent volume of the hyperventilated region.

In the case of the lungs, the region which seems to be ventilated to a greater extent is within the basal lobes (Fig.4-2), precisely where the cross-section of the lung volume is the

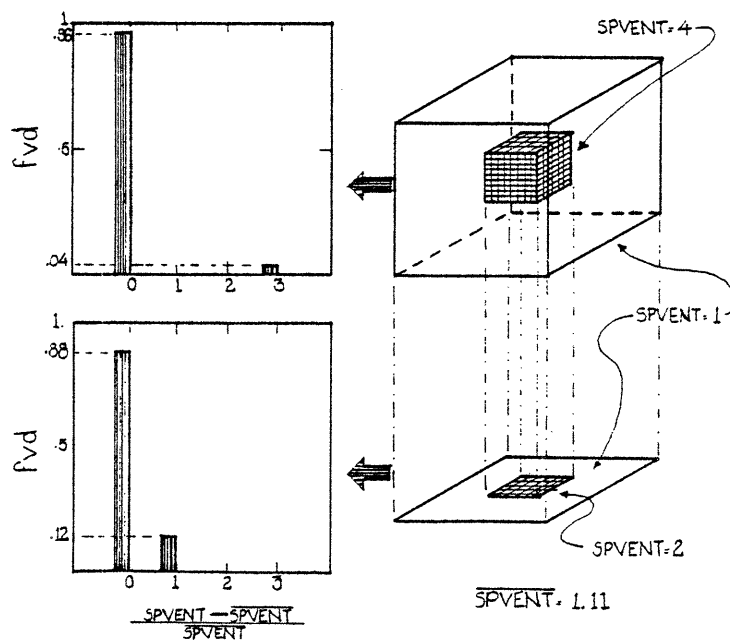


Figure 4-4: Simple example of the effect of using a two-dimensional image to generate the histograms. For explanation see text.

largest. If, for example, the hyperventilated region were only a small section around the basal lobar bronchi, from an anterior-posterior view of that region, it would seem that the total cross section of the lung was receiving the same specific ventilation. The value of such apparent specific ventilation would be equal to the mean of the actual specific ventilations across the lung, a much lower value than the specific ventilation of the hyperventilated region. In other words, the real specific ventilation of a small hyperventilated region could be much greater than the value measured from an anterior-posterior view.

Figure 4-5 presents at the left the histogram obtained from the *MTT* two-dimensional image. At the right is the type of histogram that would have been obtained from a



The Libraries
Massachusetts Institute of Technology
Cambridge, Massachusetts 02139

Institute Archives and Special Collections
Room 14N-118
(617) 253-5688

There is no text material missing here.
Pages have been incorrectly numbered.

hypothetical three-dimensional image for a lung in which the volume of the hyperventilated region is only a small fraction of the basal compartments volume .

Event though at this point it is not possible to know with certainty the actual volume of the hyperventilated region, this geometrical consideration should be kept in mind when interpreting the results.

4.2 Partially Occluded Airway

"Areas of interest" were defined for the lobe served by the obstructed airway and for the equivalent area of the opposite lung. Specific ventilations were calculated for each of these areas using the same methods described above for normal lungs.

Chapter 5

RESULTS

The results are presented in two main sections. The first section is concerned with the effects of V_t and f , during *HFV*, on overall ventilation of the lungs, as assessed by the ^{13}NN washout method. In this section an expression that can be used to select the combination of V_t and f needed to produce eucapnic ventilation, given the animal's body weight and lung volume is derived. Also, the predictions of alveolar ventilation using the classical pulmonary physiology expression for CV , where $V_t > V_D$, will be compared with the experimental results obtained for *HFV*.

The second section is concerned more specifically with the regional distribution of specific alveolar ventilation produced by *HFV*. The effects of V_t and f on different parameters related to the topographical distribution of the ^{13}NN clearance rates in normal animals initially will be shown. Later, a comparison of the effects of a partial airway obstruction on the distribution of ventilation during eucapnic *HFV* and *CV* will be presented.

5.1 Whole-lung Ventilation

5.1.1 Specific alveolar ventilation

Lung volume at *FRC*, as will be seen, is a key parameter for correlating the whole-lung specific ventilation of different animals. During protocol #1 the *FRC* measurements were not performed, and thus it is not possible to compare quantitatively the results obtained from different animals. Furthermore, since only one or two values of the $(V_t \times f)$ product were measured for each of the three E:I ratio used, the effect of frequency alone or E:I ratio can not be inferred from the set of experiments with protocol #1.

Because protocol #2 provides a more complete view of the relationships under investigation, its results will be presented first. The results obtained in protocol #1, will also be presented because they show several important trends that are consistent with the results of protocol #2.

5.1.1.1 Protocol #2

Typical results for a single dog experiment are presented in figure 5-1 where *SPVENT* is plotted vs $(Vt \times f)$.

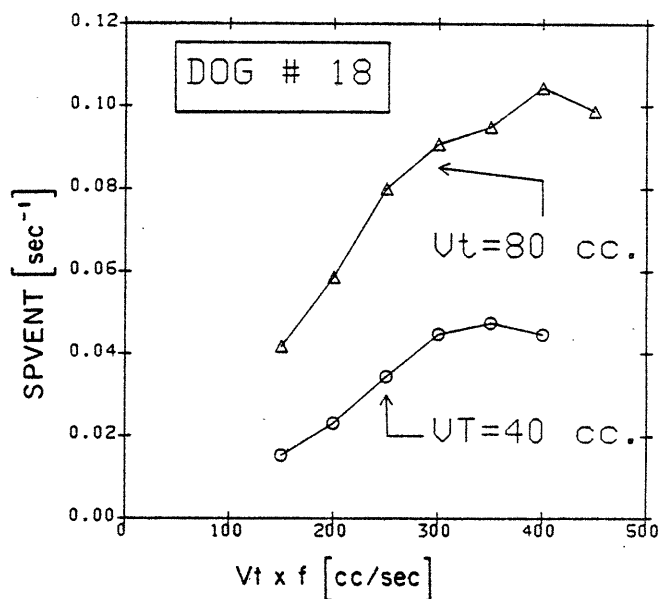


Figure 5-1:
Experimental results, from dog #18, of whole-lung *SPVENT* plotted vs the product $(Vt \times f)$ for a constant $Vt=80$ (upper curve) and $Vt=40$ cc. (lower curve). Notice the large Vt effect present for the same $(Vt \times f)$.

The Upper curve is for a Vt of 80 cc. and the lower curve for a Vt of 40 cc.. Notice the monotonic increase of *SPVENT* with frequency and the large tidal volume effect independent of $(Vt \times f)$. This type of behavior was consistent in the 6 animals studied as shown in figure

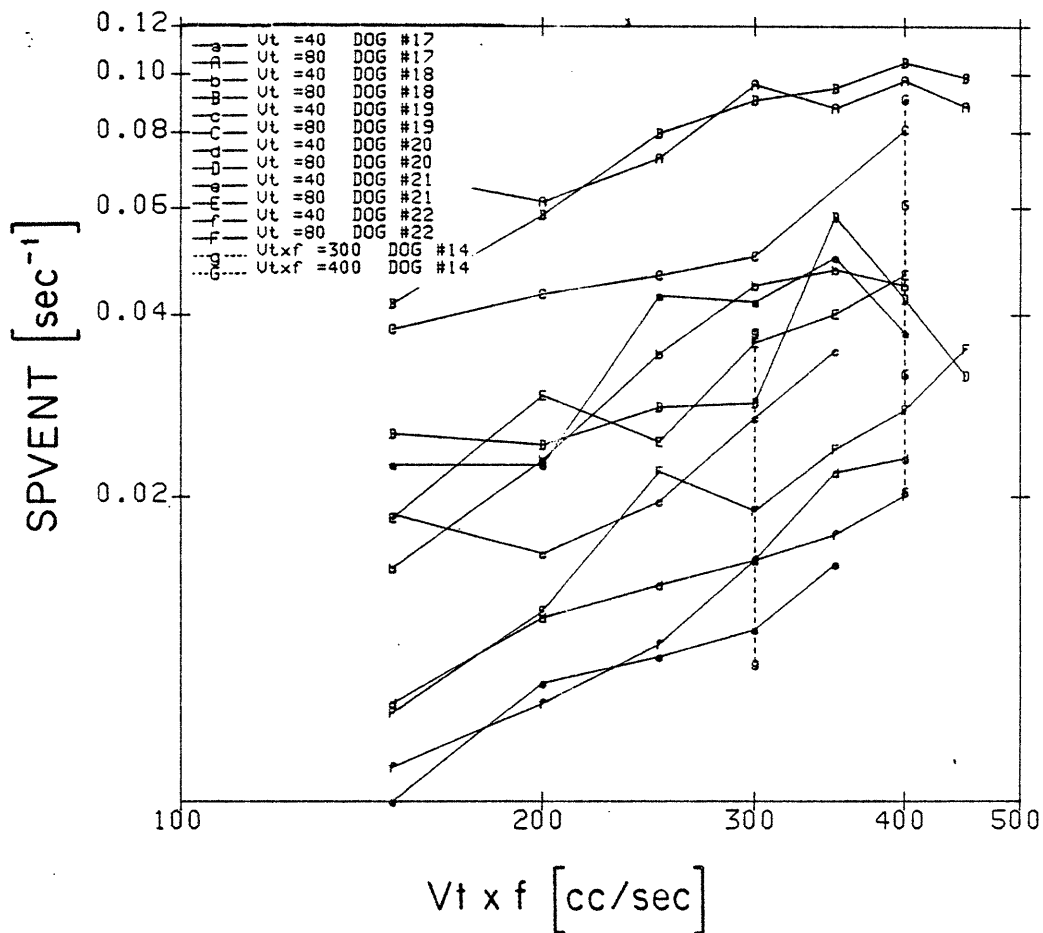


Figure 5-2:
 Experimental results, of whole-lung *SPVENT* vs the product ($Vt \times f$) from protocol #2. For each of the 6 animals there are two curves; one for a constant $Vt=40$ cc. and another for a constant $Vt=80$ cc. Although the two dotted lines ("g" and "G") are from protocol #1 they are included for comparison with fig. 5-4.

5-2 where *SPVENT* is again plotted vs $(V_t \times f)$, in log-log scales, for all animals². In assessing these results it is important to realize that they were obtained from animals of different sizes and with tidal volumes of 40 and 80 cc. It seems reasonable to expect that the animal's lung volume should have an effect in the whole-lung specific ventilation. On one hand, the definition of the *SPVENT* parameter involves a normalization by the lung volume. On the other hand, the relative size of the tidal volume, with respect to the animal lung volume, influences the depth of penetration into the lungs of the fresh gas at the end of inhalation. Furthermore, parameters characterizing the fluids of the respiratory gases, such as the Reynolds number and the Womersley parameter, are dependent on the flow velocities, which in turn scale with a power of *FRC*. Dimensional analysis would say, for geometrically similar lungs:

$$\frac{SPVENT}{f} = function\left(V_t, FRC, f, \nu, compliance, \dots\right)$$

where ν =kinematic viscosity of air= 0.15[cm²/s]. In dimensionless groups we have

$$\frac{SPVENT}{f} = function\left(\frac{V_t}{FRC}, \frac{FRC^{2/3}f}{\nu}, \dots\right)$$

Notice that the group $(FRC^{2/3}f / \nu)$ is proportional to the second power of the Womersley parameter (α^2).

In order to find the individual effects of the normalized tidal volume (V_t/FRC) and (α^2) on the whole-lung *SPVENT/f*, a multiple regression analysis was performed on the

²Because its *FRC* was measured, Dog #14 of Protocol #1 is also included. The reason for its inclusion will be explained later

experimental data³ and the following expression was obtained:

$$\left(\frac{SPVENT}{f}\right) = A_0 \left(\frac{Vt}{FRC}\right)^{A_1} \left(\frac{FRC^{2/3}f}{v}\right)^{A_2}$$

with constants:

$$\begin{array}{lll} A_0 = 4.25 & & \\ A_1 = 1.99 & (sd = .14 \quad T-VAL = 13.6 \quad SIG. LEV = .0001) & \\ A_2 = -0.14 & (sd = .12 \quad T-VAL = -1.2 \quad SIG. LEV = .23) & \end{array}$$

where:

$$\begin{array}{ll} F \text{ VALUE} = 201.22 & \\ \text{MULT REGR COEFF} = 0.91 & \end{array}$$

It is important to notice that the effect of α^2 , represented by the value of A_2 , is very small and not statistically significant. Hence, we repeated the regression analysis this time dropping the term α^2 and obtained:

$$\left(\frac{SPVENT}{f}\right) = A_0 \left(\frac{Vt}{FRC}\right)^{A_1} \tag{5.1}$$

with constants:

$$\begin{array}{lll} A_0 = 1.9 & & \\ A_1 = 2.1 & (sd = .11 \quad T-VAL = 20.0 \quad SIG. LEV = .0001) & \end{array}$$

where:

$$F \text{ VALUE} = 398.6$$

³Runs from Dog # 14, protocol #1, were also included

MULT REGR COEFF = 0.91

Figure 5-3 shows the experimental data from protocol #2 plotted now, according to the results from the dimensional analysis and equation (5.1).

Figure 5-4 presents the same data from figure 5-2 of *SPVENT* but plotted this time vs $((V_t/FRC)^{2.1}f)$ instead of $V_t \times f$. Notice that, in contrast with figure 5-2, the data from the different dogs appears to follow the same general relation and that dog #14 (dotted lines) follow closely the same relation as the rest of the animals.

5.1.1.2 Protocol #1

In this set of animals, the whole-lung *SPVENT* was found to be linearly related to V_t when the product $(V_t \times f)$ was kept constant (Fig. 5-5). This linear relationship was consistent in all dogs and with all E:I ratios and all $(V_t \times f)$ studied, as shown in figures 5-6 and 5-7. The greater scatter of the data may be attributed to the lack of normalization by *FRC* and, to the frequency effect when $(V_t \times f)$ was changed.

Notice that equation (5.1) obtained from protocol #2 can also be written as:

$$SPVENT = 1.9 \frac{(V_t \times f)}{FRC} \left(\frac{V_t}{FRC} \right)^{1.1}$$

and thus can very well explain the results from protocol #1 where *SPVENT* follows closely a linear relation with V_t when $(V_t \times f)$ is kept constant.

The actual effect of the E:I ratio alone can not be fully identified from this set of experiments for the reasons previously mentioned. However, T tests, comparing the average specific ventilations measured during the 34 runs made with $E:I > 1$ with the average of the 46 runs performed with an $E:I=1$, were performed. It was found that the mean of the measured *SPVENT* for all those runs where the $E:I > 1$, was not significantly different⁴ from

⁴In the rest of the text, 'significantly different' is defined at a significance level=.05

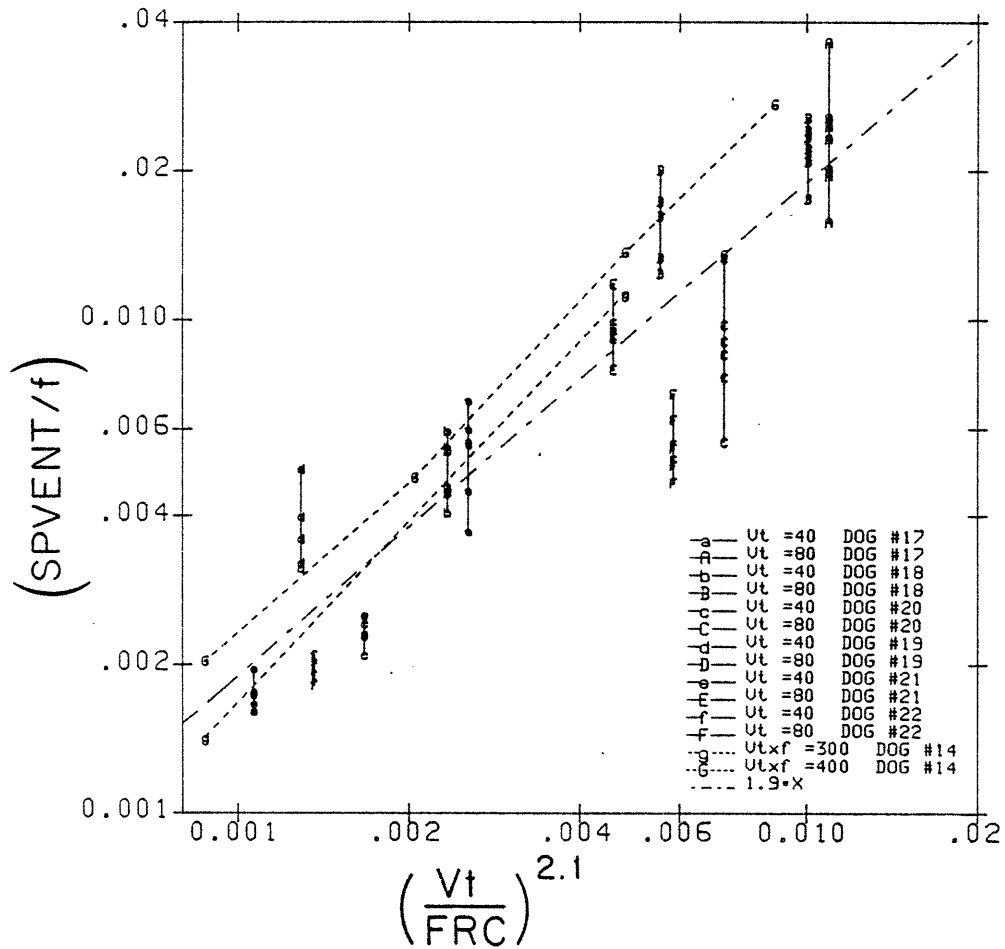


Figure 5-3:
 Experimental results for protocol #2 plotted in
 log-log scales according to the results from
 dimensional analysis

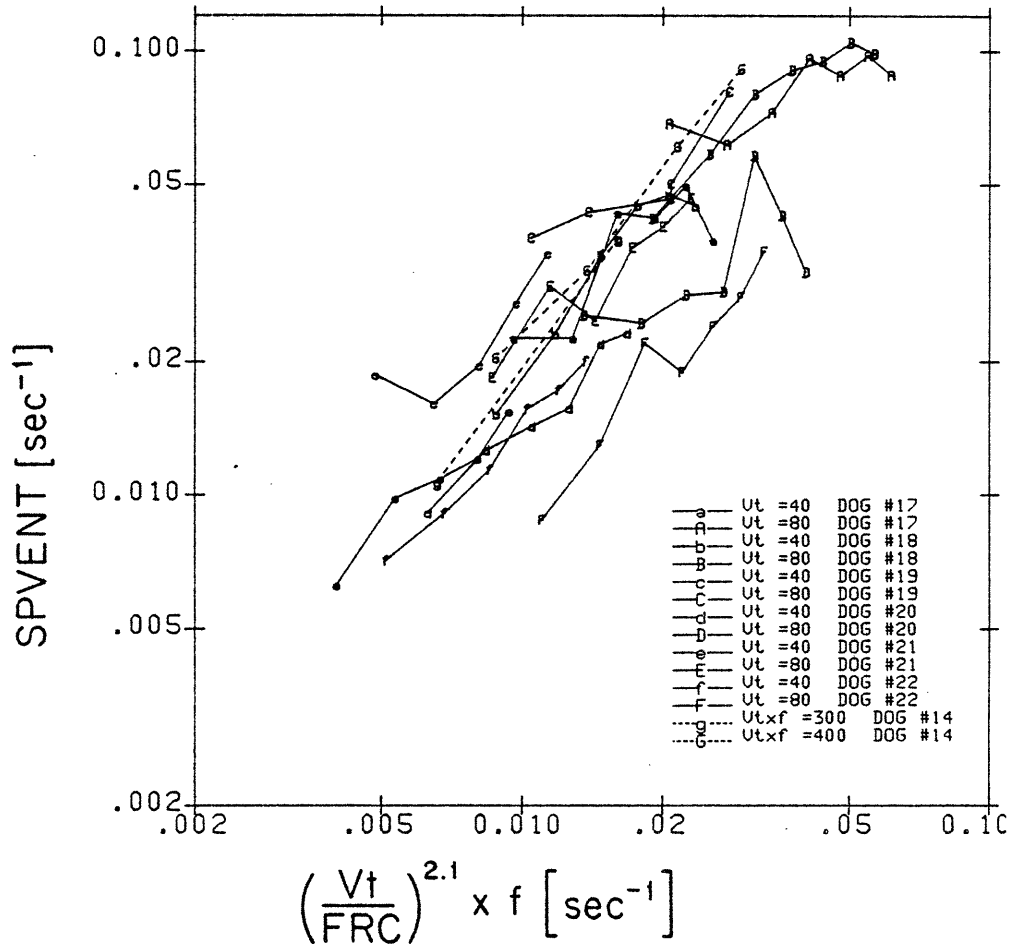


Figure 5-4:
 Same experimental results from figure 5-2
 but plotted now according to equation (5.1).

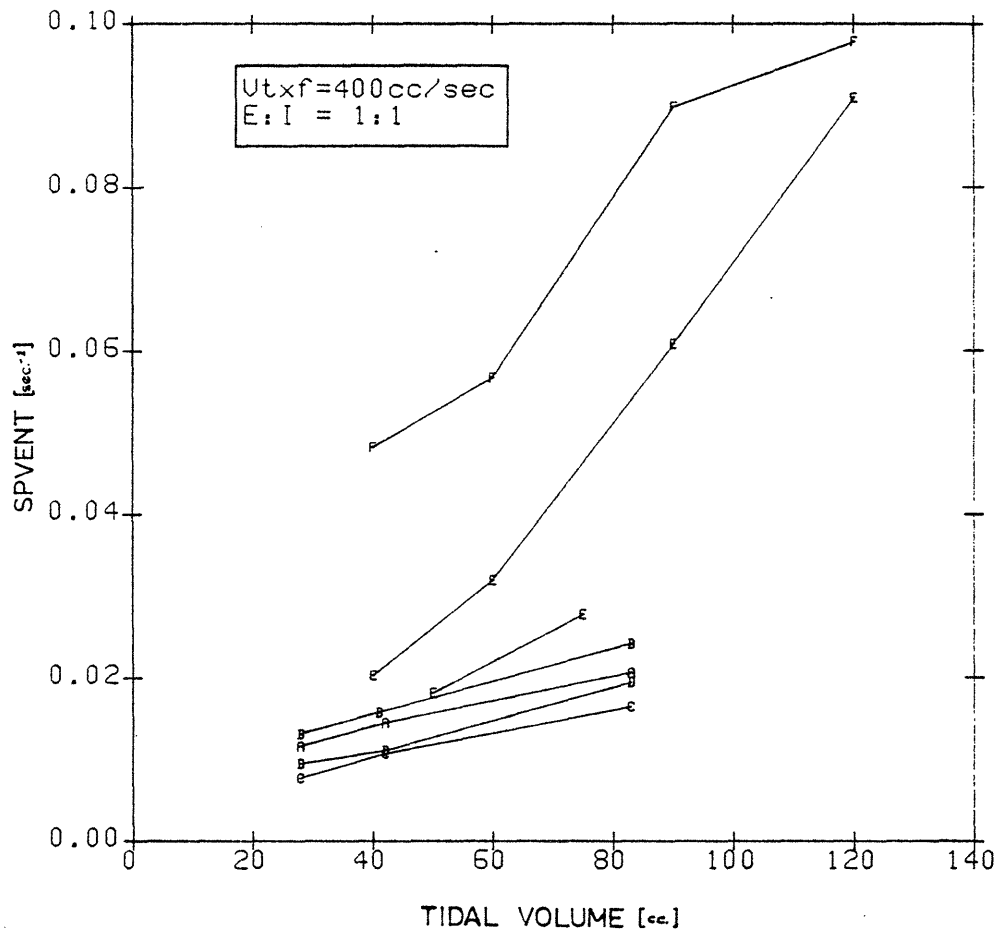


Figure 5-5:
 Experimental results from protocol #1 of whole-lung *SPVENT* vs *Vt* for 7 animals. All the runs were made with constant ($Vt \times f$) = 400 cc/sec and E:I = 1 .

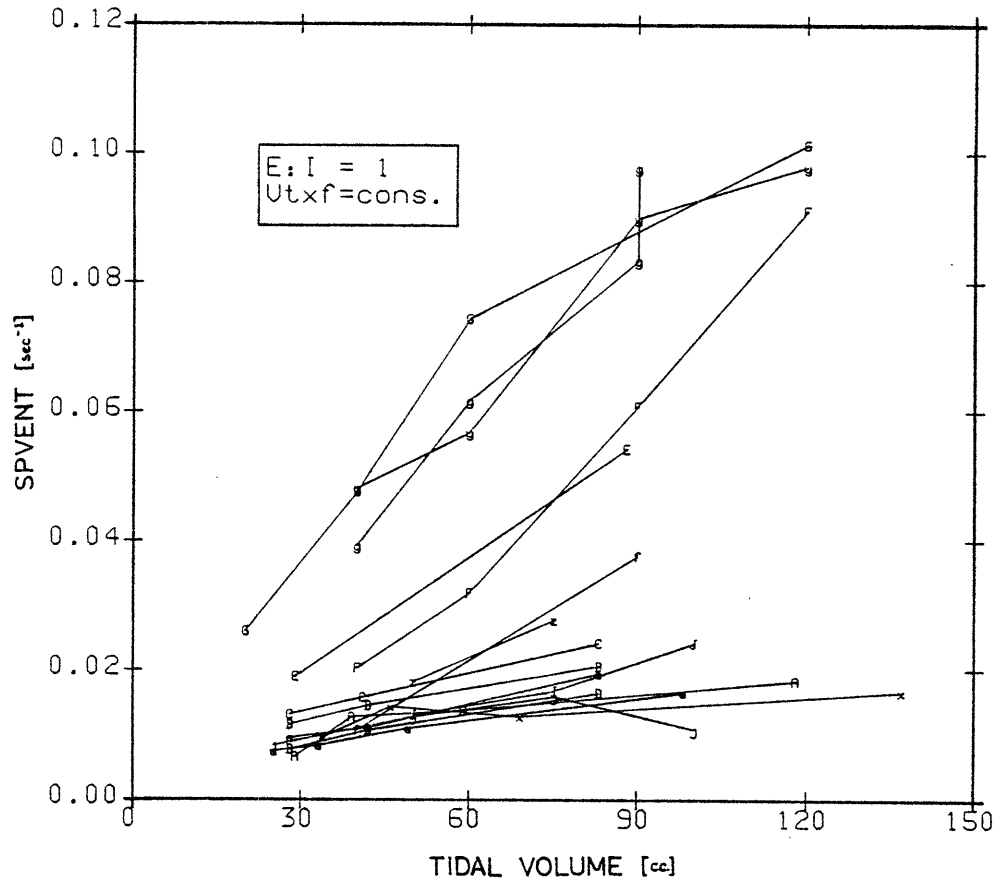


Figure 5-6:
 Experimental results of whole-lung *SPVENT* vs V_t for constant ($V_t \times f$) and $E:I=1$ for all dogs of protocol #1. Notice in all cases the linear relation between V_t and *SPVENT*

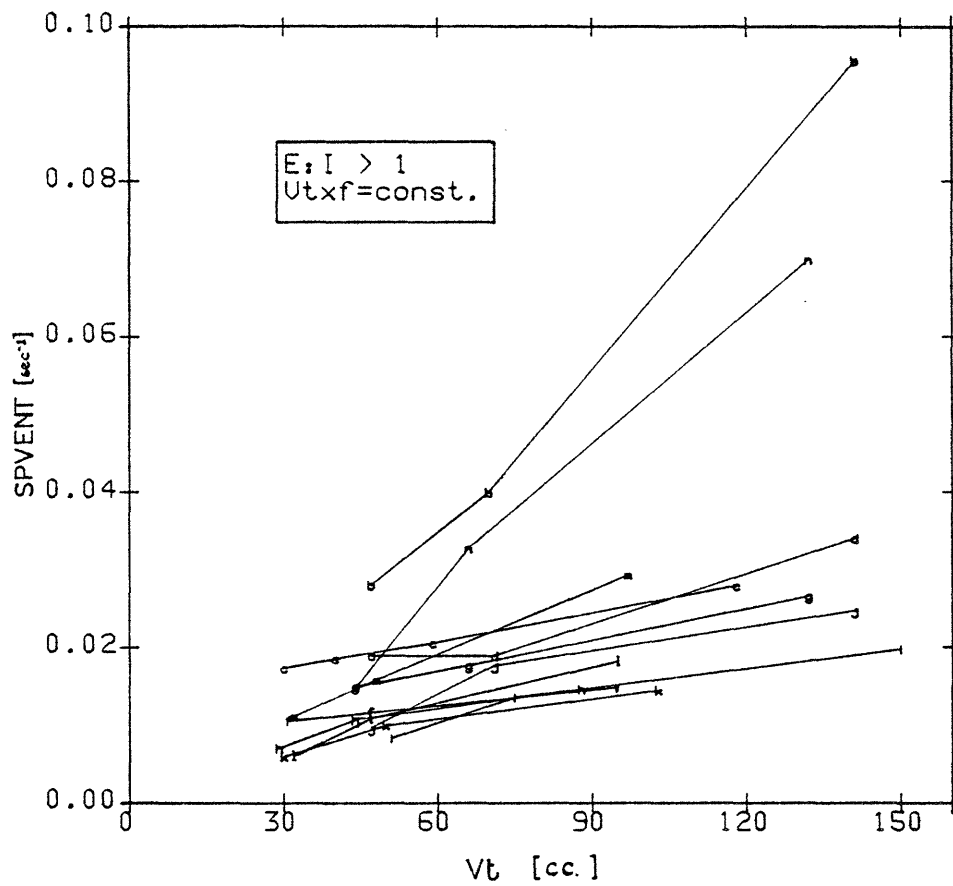


Figure 5-7:
 Experimental results of whole-lung SPVENT vs V_t for constant ($V_t \times f$) and $E:I > 1$. There was not a substantial difference between these results and those of figure 5-6

the mean from all those runs with $E:I=1$, in spite of the fact that the two populations had similar means of V_t and f (fig. 5-7). This result, however, is not conclusive, since the FRC volumes of the animals were not measured and it is not known whether the mean of this parameter was statistically similar for both groups.

5.1.2 Specific Ventilation and CO_2 transport.

So far, the relationship between $SPVENT$ and V_t , f , and FRC has been explored. In this section, evidence supporting the relevance of $SPVENT$ for predicting the arterial PCO_2 status of the animal during HFV will be presented.

Because the whole-lung $SPVENT$ is equivalent to the mean alveolar ventilation per unit of lung volume, the total alveolar ventilation per unit of body weight ($VENT$), produced with HFV , can be calculated as:

$$VENT = SPVENT \times \frac{FRC}{BW} \quad (5.2)$$

where

$SPVENT$ = specific alveolar ventilation (1/sec)

FRC = volume of lung at FRC (cc.)

and

BW = body weight (kg.)

Figure 5-8 presents a log-log plot of the arterial blood PCO_2 , measured four minutes after the onset of HFV , vs $VENT$ for all the runs performed in protocol #2. The best fit straight line for these data yields the expression:

$$PaCO_2 = (42.6 \pm 1.02) \times (VENT)^{-.44 \pm .028} \quad (5.3)$$

with a correlation coeff $R = 87.86$

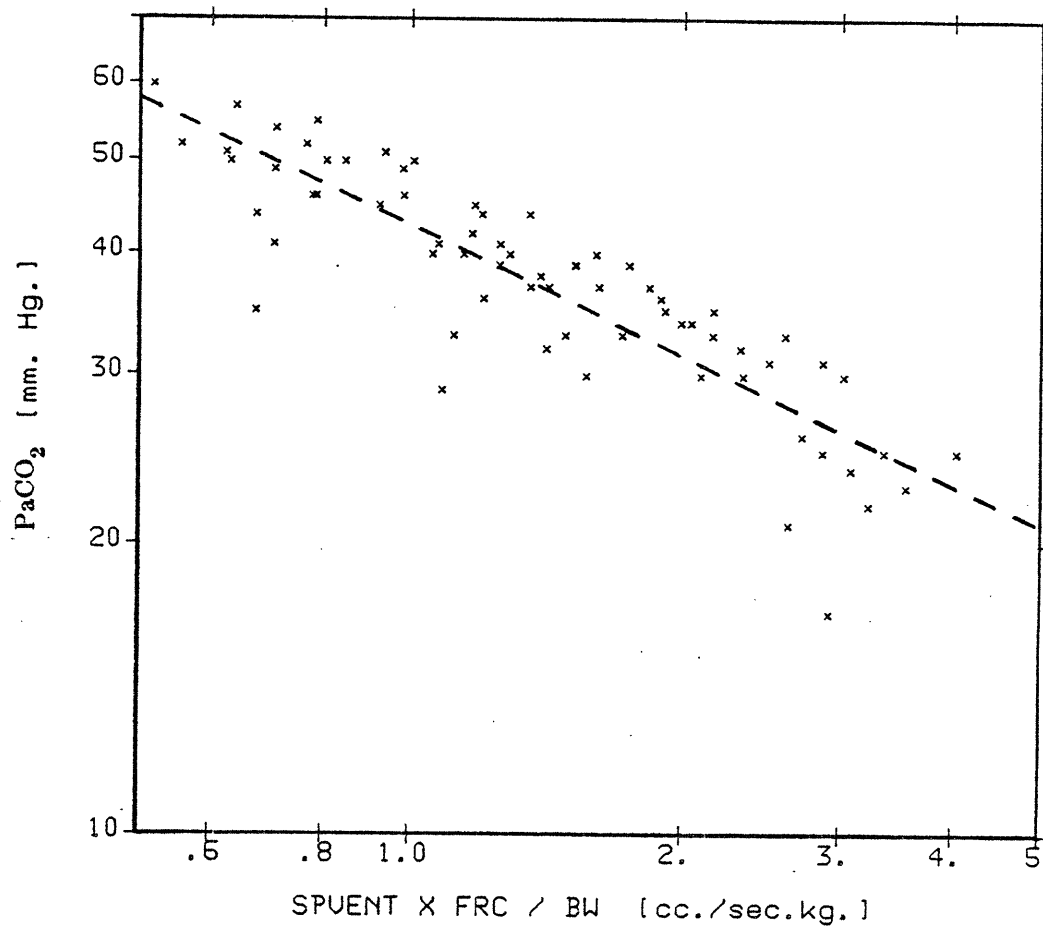


Figure 5-8:
 Log-log plot of arterial blood PCO₂,
 measured after four minutes of HFV, vs total
 alveolar ventilation per kg for all dogs of
 protocol #2. The best fit straight line is also
 included

Because 4 minutes is a short time to establish an equilibrium in the CO₂ storage compartments of the animal's body, most of the PaCO₂ measurements do not reflect the steady state values that would have been reached if an equilibrium had been allowed to occur

However, since the conventional ventilation that preceded the washout with *HFV* was set at normocapnea with an average $\text{PaCO}_2 = 37$ mm. Hg. (sd.=5.4 mm. Hg.), for this value of PaCO_2 the system was in fact at steady state. Thus, the calculated VENT from equation (5.3), for a $\text{PaCO}_2=37$ mm Hg., reflects the total ventilation per kg. needed to maintain eucapnea. This value is $\text{VENT}_n=1.38$ (cc./sec.kg).

This measurement of VENT_n , obtained from the ^{13}NN washout data, will now be compared to the value calculated from available data for the basal metabolism of dogs. In order to accomplish this goal, the alveolar ventilation needed for eucapnea can be calculated from the O_2 consumption for dogs ($\text{VO}_2=330$ [cc./kg.Hr.] (Altman and Pitmer, 1971)) using the well known equation of pulmonary physiology⁵:

$$\text{VENT}_n = \text{VO}_2 \times R \times \text{FA}_{\text{CO}_2} \quad (5.4)$$

where:

FA_{CO_2} = alveolar fraction concentration of CO_2

R = respiratory exchange ratio

so assuming a normal $R=.8$ and using $\text{FA}_{\text{CO}_2}=.052$ for a $\text{PaCO}_2=37$ mm. Hg. the value of $\text{VENT}_n = 1.41$ cc/(kg..sec.).

The fact that the values of VENT_n obtained from Eq. (5.3) and Eq. (5.4) are so similar strongly supports the validity of the measurement of alveolar ventilation with the ^{13}NN washout method.

⁵ (West, 1979)

5.1.3 The HFV Equation.

From equations (5.1) and (5.2) and using the value of $VENT_n$ obtained from Eq.(5.3) for a $PaCO_2=37$, the following expression is obtained:

$$V_t^{2.1} \times f = .73 \times FRC^{1.1} \times BW \quad (5.5)$$

This expression allows one to set the parameters of the HFV ventilator so that normocapnea is achieved. Notice that both the subject's body weight and lung volume at FRC are key parameters for choosing the normocapnic pair of V_t and f .

5.1.4 Efficiency of HFV and CV

Since the empirical Eq.(5.1) predicts the alveolar ventilation produced by HFV, this can now be compared with the predictions from the classical analysis for conventional ventilation.

Let us define the efficiency of ventilation as:

$$\eta = \frac{\text{Alveolar Ventilation}}{\text{Oscillatory Flow}} \quad (5.6)$$

where alveolar ventilation can be defined as the equivalent flow of fresh gas that is participating in the gas exchange and the oscillatory flow is the product ($V_t \times f$) delivered by the apparatus.

From classical respiratory physiology for CV the alveolar ventilation (\dot{V}_{alv}) is:

$$\dot{V}_{alv} = (V_t - V_d) \times f$$

where V_d is the volume of the anatomic dead space. Therefore,

$$\eta_{CV} = (1 - 1/(V_t/V_d)) \quad (5.7)$$

This equation is only valid for $V_t \gg V_d$

Since alveolar ventilation is also:

$$\dot{V}_{alv} = SPVENT \times FRC \quad (5.8)$$

referring now to HFV , combining equation (5.8) with equation (5.1) yields:

$$\dot{V}_{alv} = 1.9 \left(\frac{V_t}{FRC} \right)^{1.1} \times V_t \times f^{0.88} \quad (5.9)$$

and so

$$\eta_{HFV} = 1.9 \left(\frac{V_t}{FRC} \right)^{1.1} \quad (5.10)$$

This last expression, evaluated in the range of V_t / FRC reported here and replacing the value of V_d by,

$$V_d \approx .08 \times FRC \text{ (Altman and Pitmer, 1971)}$$

yields:

$$\eta_{HFV} \approx .12 \times (V_t/V_d) \quad (5.11)$$

which is valid for $(1/4V_d) < V_t \leq V_d$ since the anatomic dead space of our animals was around 80cc. and our smaller tidal volume was 25cc.

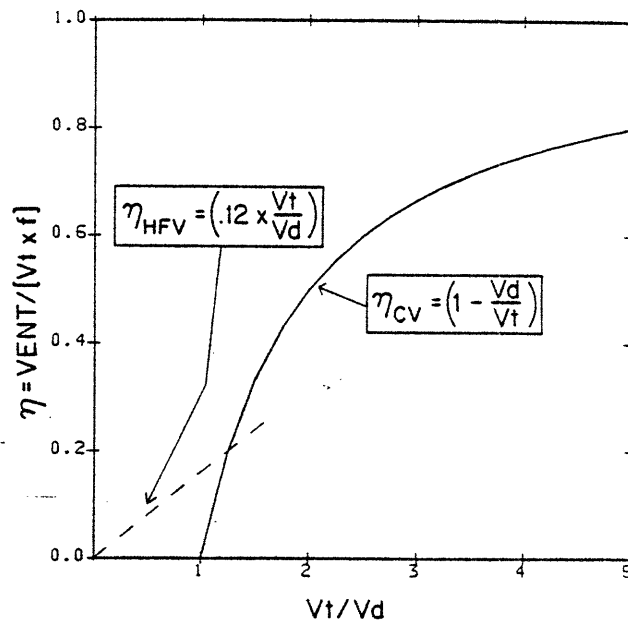


Figure 5-9:
Efficiency (η) of HFV and CV plotted vs
(V_t/V_d). For explanations see text

Equations (5.7) and (5.11) are plotted together in figure 5-9. Notice that the efficiency of CV is greater than that of HFV at a $V_t/V_d \approx 1.15$. Furthermore, the efficiency of HFV is only 0.1 for $V_t/V_d=0.5$.

5.2 Regional Distribution of Ventilation

So far, this report has presented only results related with the ventilation of the lung as a whole. In this section the effects of V_t and f on the regional distribution of the specific alveolar ventilation will be reported.

5.2.1 MTT Functional Images

The *MTT Visual Images* provide a qualitative assessment of the regional distribution. Here aswell, the lighter regions represent the areas with longer *MTT* and the darker regions, represent the areas with shorter *MTT*. Care must be taken when interpreting such images, since they are dependent on the setting of the contrast and the brightness levels of the display screen. In order to deal with this problem, the contrast and brightness were set at the same level for all the images.

Figure 5-10 presents, as an example, the *MTT* images obtained from dog #16 from Protocol #1.

Each image corresponds to a run with particular settings for V_t and f . All runs, however, were made with the same $(V_t \times f)$ product. The images near the top are from runs with a higher frequency but a proportionately lower tidal volume than the ones towards the bottom.

Notice that for the smaller tidal volumes (and thus larger frequencies) the distribution looks very homogeneous with only a small central region of hyperventilation. For the largest tidal volumes, however, the hyperventilated region increases in size and seems to cover most of the base of the lungs.

Figure 5-11 presents typical results from protocol #2. In this case the images near the top correspond to the higher frequencies and the ones near the bottom to the lower frequencies. In the right column, are the runs made with a constant $V_t=80$ cc and in the left

DOG #16

E:I=1

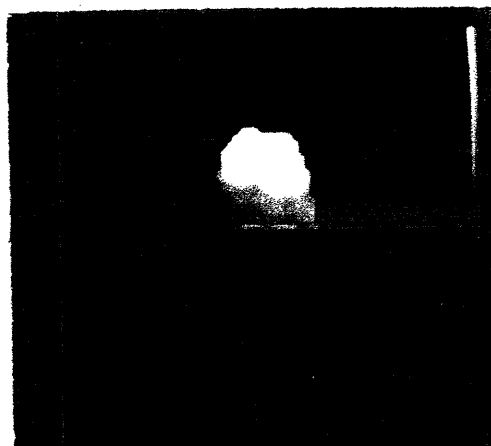
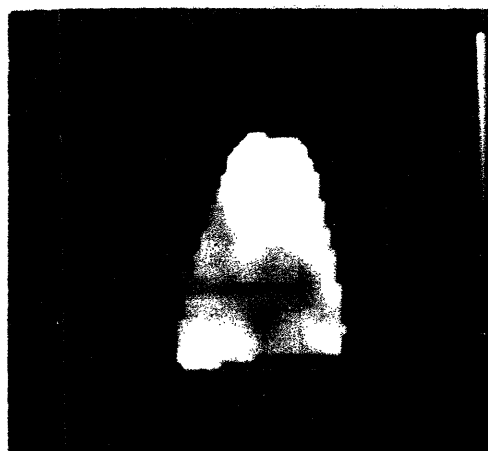
 $V_t \times f = 200 \text{ cc./sec.}$ $V_t = 100 \text{ cc}$ $f = 2 \text{ Hz}$  $V_t = 75 \text{ cc}$ $f = 2.8 \text{ Hz}$  $V_t = 50 \text{ cc}$ $f = 4 \text{ Hz}$  $V_t = 25 \text{ cc}$ $f = 8 \text{ Hz}$ 

Figure 5-10: MTT images for dog #16. Each image was obtained from a run with particular settings for V_t and f but all have the same $(V_t \times f) = 200$ cc/sec.. Notice that the larger tidal volumes (images near the top) preferentially ventilated the bases of the lung.

DOG #20

E:I=1

$V_t = 40$ cc

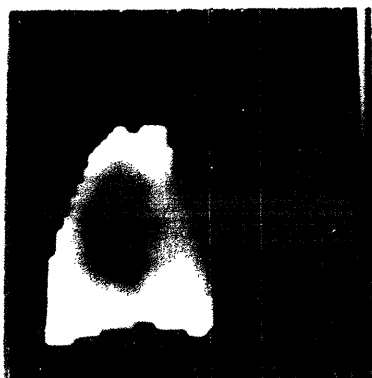
$V_t = 80$ cc



$V_t \times f = 400$ cc/sec



$V_t \times f = 250$ cc/sec



$V_t \times f = 150$ cc/sec

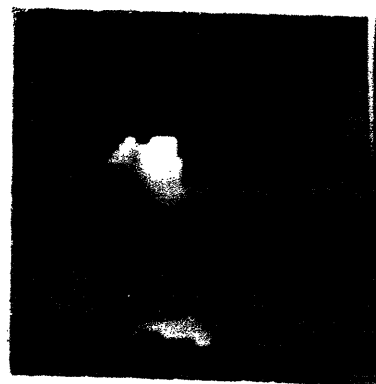


Figure 5-11:

Set of MTT images from protocol #2. The left column contains the ones for the runs made with $V_t=40$ cc. and the right column the ones for the runs made with $V_t=80$ cc.. Each row has the same $(V_t \times f)$ product with the higher frequencies located nearer the top.

column the runs made with a constant $V_t=40$ cc. The tidal volume effect at constant $(V_t \times f)$ product is found by comparing right with left contiguous images.

Notice that in this case the changes in frequency don't seem to affect the distribution of ventilation as dramatically as the tidal volume did in protocol #1.

The qualitative results obtained by visual inspection of these images are confirmed by the following analysis.

5.2.2 Quantitative analysis

The effects of V_t and f on the regional distribution of specific ventilation were quantified in two ways:

1. with the spread of the regional ventilation distribution for the entire lung (*SIGMA*), which gives an overall parameter of the ventilation homogeneity; and
2. with the ratios of *RIGHT/LEFT* and *APEX/BASE* of the regional specific alveolar ventilations, which define the relative differences in the magnitude of the ventilation to regions previously chosen.

These three parameters were plotted vs V_t for constant $(V_t \times f)$ and E:I ratio in the runs of protocol #1 and vs $(V_t \times f)$ for constant V_t in the runs of protocol #2. For both protocols the basic analysis consisted on fitting straight lines to the resulting curves by the least square method and to compare the average of the calculated slopes with zero, using the Student's t-distribution at a significance level of .05.

Each of the individual experimental parameters will be discussed separately later but, at this point, it is convenient to present the results from the statistical analyses summarized in table 5-I.

This table has three main columns, one for each respective parameter (*SIGMA*, *BASE/APEX*, and *RIGHT/LEFT*), and five main rows. The first main row contains the mean and standard deviation of the parameter in question taken from all the runs. The following

SUMMARY OF RESULTS FOR ALL DOGS

	SIGMA	BASE / APEX	RIGHT / LEFT
MEAN FOR ALL RUNS	0.200	1.290	1.1
St. Deviation	0.059	0.065	0.1

PROTOCOL #1			
E:I=1			

MEAN OF "Y"	0.215	1.359	1.065
X VARIABLE	TIDAL VOLUME	TIDAL VOLUME	TIDAL VOLUME
X RANGE	20 - 140 (cc.)	20 - 140 (cc.)	20 - 140 (cc.)
MEAN SLOPE	0.0012	0.0073	0.00176
ST.DEV OF SLOPE	0.0011	0.0050	0.00154
SLOPE = 0.	YES	YES	YES
(DELTA Y)/(Y MEAN)	0.68	0.64	0.20

PROTOCOL #1			
E:I>1			

MEAN OF "Y"	0.181	1.34	1.069
X VARIABLE	TIDAL VOLUME	TIDAL VOLUME	TIDAL VOLUME
X RANGE	20 - 140 (CC.)	20 - 140 (CC.)	20 - 140 (CC.)
MEAN SLOPE	0.0013	0.007	----
ST.DEV OF SLOPE	0.0002	0.004	----
SLOPE = 0.	YES	YES	----
(DELTA Y)/(Y MEAN)	.87	0.64	----

PROTOCOL #2			
Vt = 80 cc			

MEAN OF "Y"	0.199	1.291	1.145
X VARIABLE	FREQUENCY	FREQUENCY	FREQUENCY
X RANGE	2 - 5.5(HZ.)	2 - 5.5(HZ.)	2 - 5.5(HZ.)
MEAN SLOPE	0.0054	0.0330	-0.0324
ST.DEV OF SLOPE	0.0338	0.0377	0.0378
SLOPE = 0.	NO	YES	NO
(DELTA Y)/(Y MEAN)	0.094	0.089	-0.099

PROTOCOL #2			
Vt = 40 cc.			

MEAN OF "Y"	0.185	1.135	1.126
X VARIABLE	FREQUENCY	FREQUENCY	FREQUENCY
X RANGE	4 - 10 (Hz)	4 - 10 (Hz)	4 - 10 (Hz)
MEAN SLOPE	-0.0124	0.0218	-0.0110
ST.DEV OF SLOPE	0.0184	0.0206	0.03784
SLOPE = 0.	NO	YES	NO
(DELTA Y)/(Y MEAN)	-0.40	0.12	-0.06

Table 5-I:
Summary of the statistical analyses for the regional ventilation parameters. For explanation see text

four main rows contain the results from statistical analysis of the runs from:

1. Protocol #1 with $E:I=1$
2. Protocol #1 with $E:I>1$
3. Protocol #2 with $V_t=40$ cc.
4. protocol #2 with $V_t=80$ cc.

Each of these four main rows contains:

1. The mean of the parameter listed in the column heading (Mean of "y").
2. The independent variable used in the specific protocol (X variable).
3. The range of values given to the independent variable (Range of x).
4. The mean of the slopes obtained with the line fitting (Mean slope).
5. The standard deviation of the slopes (St. Dev of Slope).
6. The result of the null hypothesis test at a significance level of .05 (Null Hypothesis).
7. The mean fractional change in the corresponding distribution parameter with respect to its mean value, caused by a full range variation of the independent variable. ($\Delta Y / \text{Mean } Y$)

As an example, the *BASE/APEX* ratio of specific ventilation had a mean value of 1.29 for all runs. For the runs of protocol 2 with $V_t=40$ the mean of the *BASE/APEX* parameter was 1.135 and the slope of the regression lines was .0218 sec., which is significantly different from zero. This means that an increase of frequency from 4 to 10 Hz produced an average increase of about 12% around a mean value of 1.14.

5.2.2.1 Spread of Specific Ventilation Histograms

In figure 5-12, the spread of the histograms of specific ventilation, corrected for the measurement error, (*SIGMA*) is plotted vs tidal volume for all the experiments of protocol #1 with $E:I=1$. In this graph each curve is made from runs where the product ($V_t \times f$) was kept at a constant value while V_t was changed. The value of (*SIGMA*) increases with V_t with

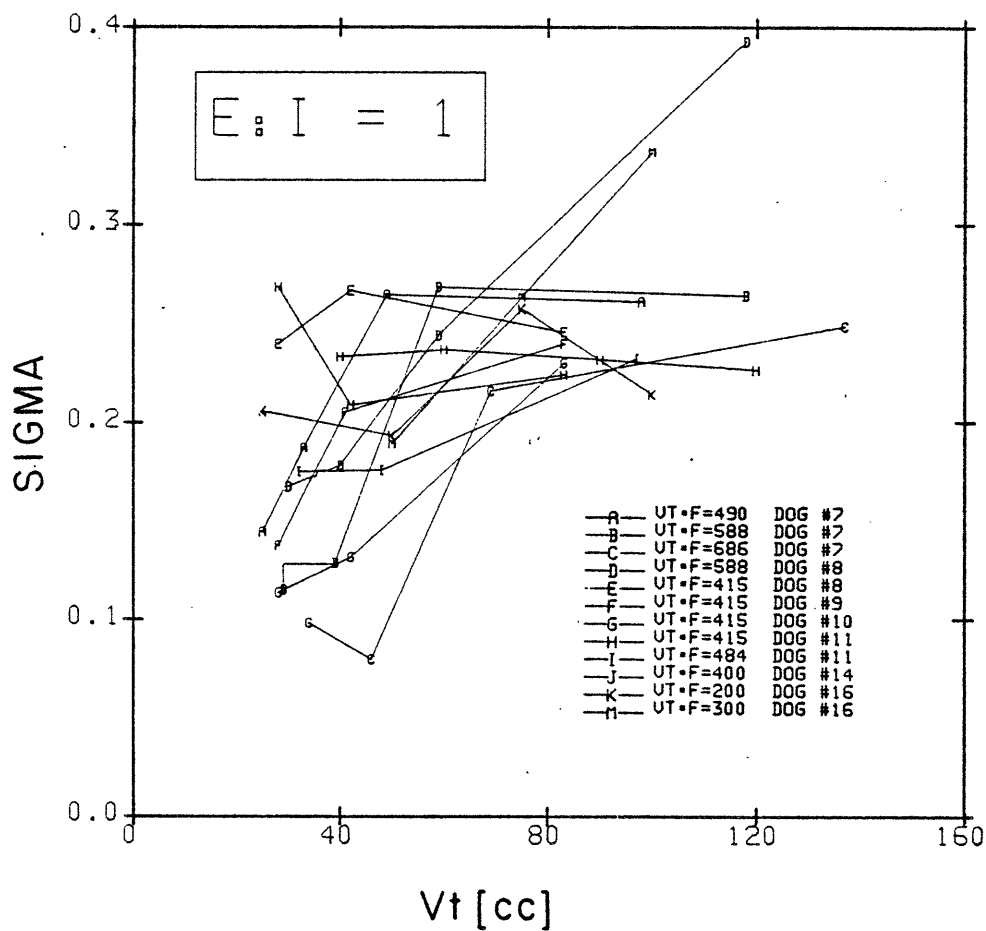


Figure 5-12:
 Experimental results of *SIGMA* vs *Vt* for all experiments of protocol #1 with $E:I=1$. Each curve is made from runs where the product ($Vt \times f$) was kept constant while *Vt* was changed.

a slope significantly greater than zero. A change of V_t from 20 cc to 140 cc. increased the spread of the normalized variations of regional specific ventilation by 68% around a mean value of .215.

The mean value of $SIGMA$ from the runs of protocol #1 with $E:I > 1$ was not significantly different from those with $E:I=1$.

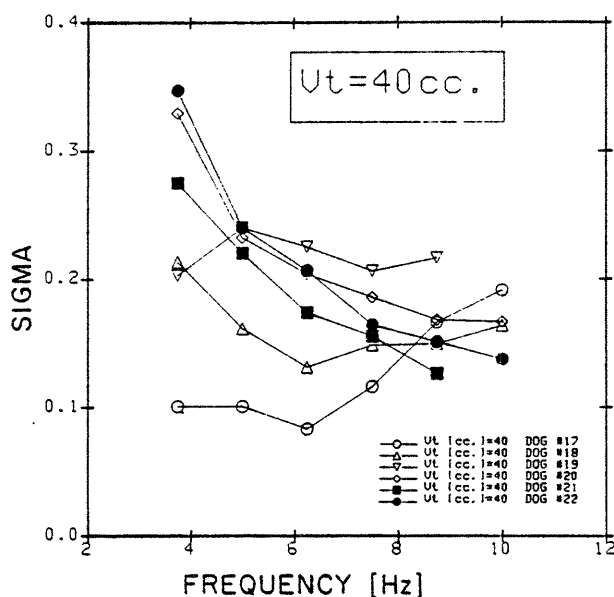


Figure 5-13:
Experimental results of ($SIGMA$) vs f for all experiments in protocol #2 with a $V_t=40$ cc. Each curve corresponds to a different animal

Frequency did not have the same effect in each of the dogs of protocol #2. Figure 5-13 is a plot of the ($SIGMA$) vs f for all experiments in this protocol with a tidal volume of 40 cc.. Similar results were obtained for the runs made with a $V_t=80$ cc.. The average of the slopes of the regression lines was not significantly different from zero for either of the tidal volumes studied. However, the magnitude of these slopes had a negative correlation with the animals' FRC ($R = -.628$ for $V_t=80$ and $R = -.677$ for $V_t=40$). This suggests that a change in frequency had an effect on the spread of the distribution histograms that was related to the FRC volume of the animal. In other words, an increase in frequency at a

constant V_t tended to decrease the spread of the $SPVENT$ histograms for the larger animals while the same change in frequency tended to increase it for the smaller animals.

5.2.3 Regions of interest

Figure 5-14 presents typical results for a typical set of three runs with the same $(V_t \times f)$ in protocol #1. Each curve represents the $SPVENT$ of each of the previously defined four regions of interest. Notice that the increase in tidal volume primarily affects the ventilation of the bases while the ventilation of the apex increases to a lesser degree. Also, notice that the right apex and the right base have a larger specific ventilation than the left apex and left base, respectively. This result was not obvious from the computer-generated pictures.

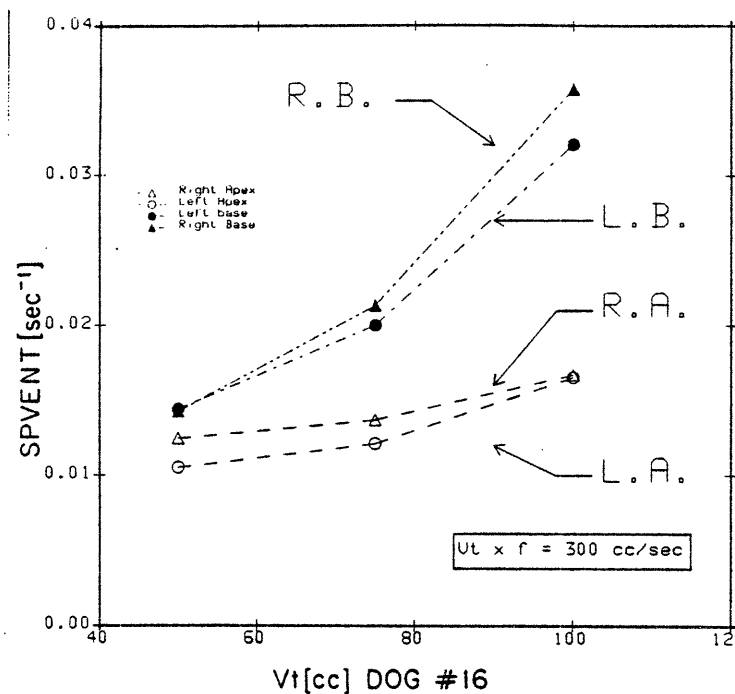


Figure 5-14:
Regional $SPVENT$ vs V_t for a set of three runs from the same dog at a $(V_t \times f) = 300 \text{ cc/sec}$. Each curve corresponds to a different region. (RA=right apex, LA=left apex, RB=right base, LB=left base) Notice that the increase in V_t produced a preferential increase in the ventilation of the bases.

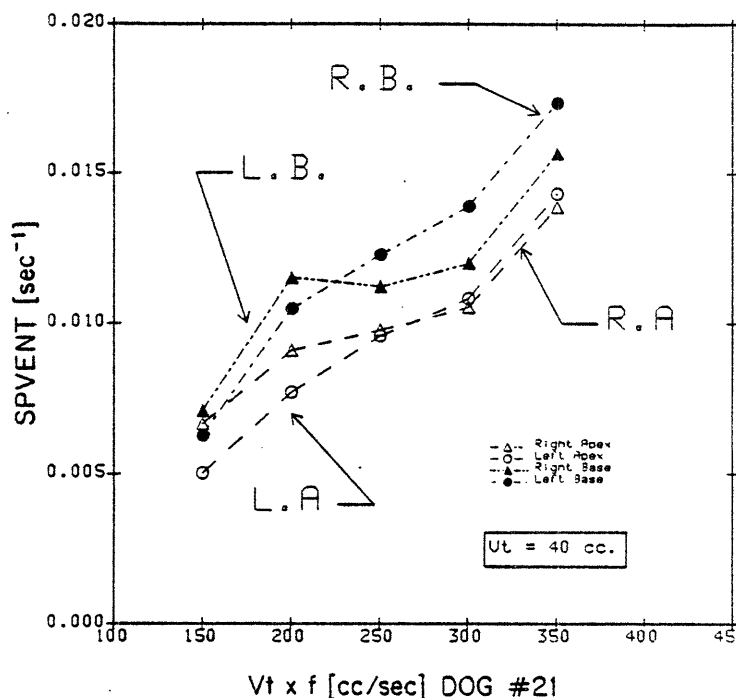


Figure 5-15:
Regional $SPVENT$ vs $(V_t \times f)$ for a set of five runs from dog # 21 where V_t was kept constant at 40cc.. Each curve is for each of the four different regions defined in fig(5-14). Notice that in this case, the increase in f produces a more distributed increase in $SPVENT$ among the different compartments than the increase of V_t at constant $(V_t \times f)$.

Figure 5-15 is a plot of regional $SPVENT$ vs $(V_t \times f)$ for a set of runs in protocol #2 with $V_t=40$. Notice that here the increase of frequency causes a more similar change in all four regions in contrast with the results from protocol #1 (5-12), where V_t was changed at a constant $(V_t \times f)$. The effects of V_t and f on the distribution of ventilation were grouped into Right vs Left lungs and Apical vs Basal regions and presented in the following sections.

5.2.3.1 Right Lung vs Left Lung Specific Ventilation

Figure 5-16 shows the ratio of the specific ventilation for the right lung to that for the left lung ($RIGHT/LEFT$) plotted against tidal volume for different products of $(V_t \times f)$. The results pertain to all dogs of protocol #1 where $E:I=1$. Notice that at the smaller V_t the

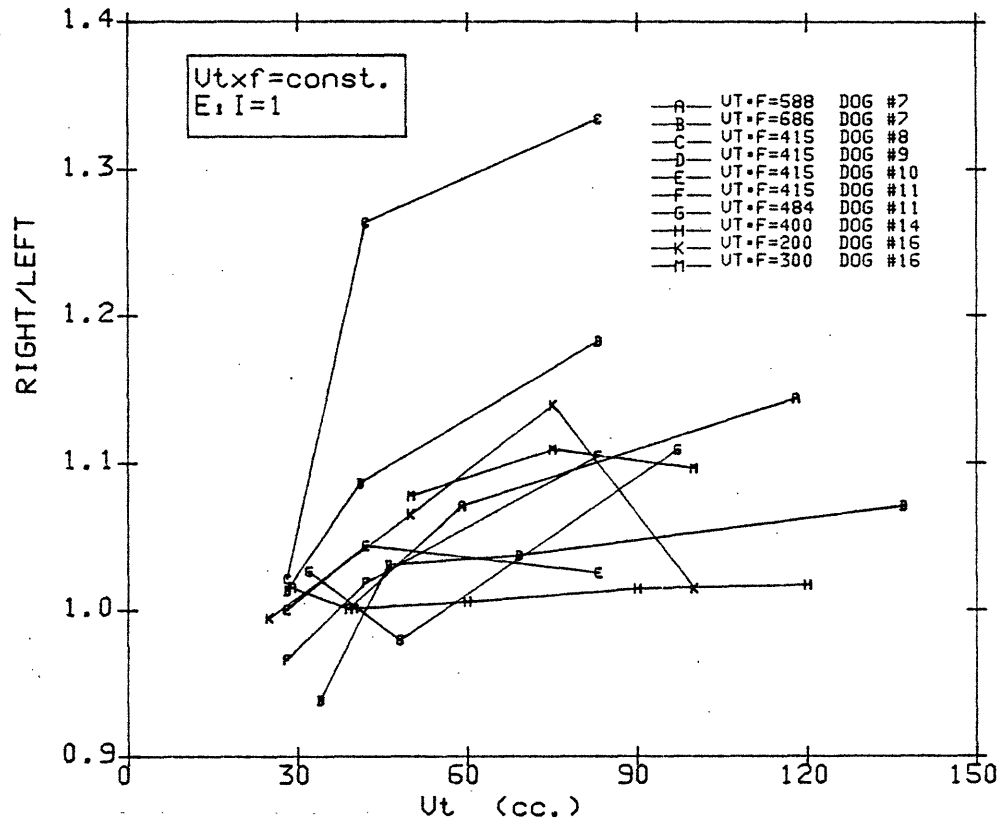


Figure 5-16:
 Experimental results, for all runs in protocol #1
 where $E:I=1$. Here, the ratio of the specific
 ventilation for the right lung to that to the left
 lung $RIGHT/LEFT$ is plotted vs V_t . Each
 curve corresponds to a single animal at a constant
 ($V_t \times f$) and $E:I$

ratio is around unity but it increases significantly for the larger tidal volumes. The specific ventilation of the right lung averaged approximately 6.5% larger than the one of the left lung over the tidal volume tested. The effect of increasing V_t from 20 to 140 cc., was to increase the *RIGHT/LEFT* ratio an average of 20% around a mean value of 1.065.

The results for $E:I > 1$ in protocol #1 were not significantly different from the ones for $E:I = 1$, with respect to the *RIGHT/LEFT* ratio.

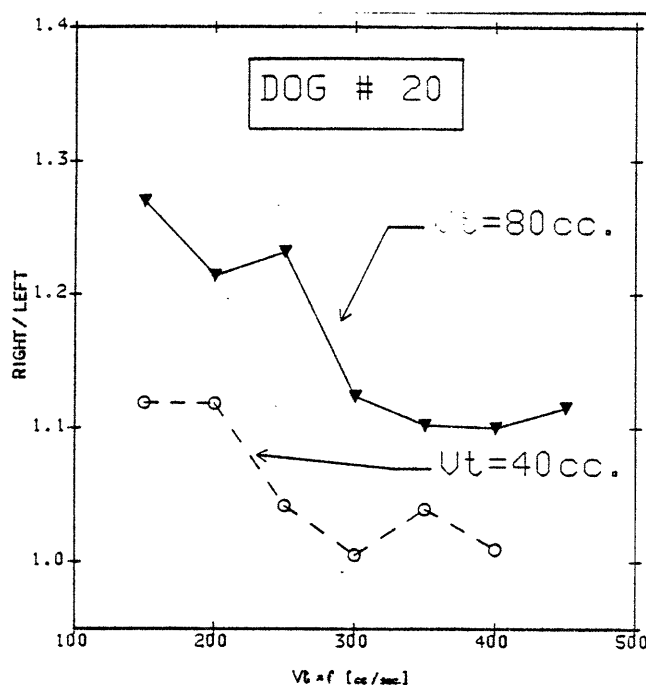


Figure 5-17:

Example of experimental results from dog #20 of protocol #2 where the *RIGHT/LEFT* ventilation ratio is plotted vs $(V_t \times f)$. For the runs of each curve the V_t was kept constant at 80cc. (triangles) and 40cc. (circles).

Figure 5-17 presents an example of the results from an experiment of protocol #2. Here, the *RIGHT/LEFT* ratio is plotted vs $(V_t \times f)$ for the two values of tidal volume studied. Notice that the data for $V_t = 80$ lie generally above the data for $V_t = 40$ cc., in agreement with equivalent findings from protocol #1. Although the effects of frequency for the individual dogs of protocol #2 were often appreciable, the mean of the slopes of the best fit

straight lines was not significantly different from zero for either of the two tidal volumes investigated. However, the magnitude of these slopes is negatively correlated with the animal's lung volume at *FRC* ($R=-.889$ for $V_t=40$ cc. and $R=-.886$ for $V_t=80$ cc.). This means that in the larger animals, increases in frequency tend to decrease the differences in specific ventilation between the right and left lungs while in the smaller dogs (ie. the relatively larger flow rates and tidal volumes) the differences between the *SPVENT* of both lungs are increased.

5.2.3.2 Basal vs Apical Ventilation

Figure 5-18 presents the ratio of the specific ventilation of the basal regions to that for the apical regions plotted against V_t for constant ($V_t \times f$) values and for all runs of protocol #1 where $E:I=1$. Notice that the ratio is greater than one for all tidal volumes and that it generally increases with the tidal volume. The mean of the slopes of the regression lines was positive. This means that for a change in tidal volumes from 20 to 140 cc. the *BASE/APEX* ratio changed by 64% around its mean value of 1.359.

For the runs where $E:I>1$ neither the mean slope of the regression lines nor the mean value of the *BASE/APEX* ventilation ratio is significantly different from the results with $E:I=1$.

A plot of the basal over apical specific ventilation ratio against ($V_t \times f$) for a typical dog of protocol #2 is presented in figure 5-19. Notice that the data for a tidal volume of 80 cc. lies above the data for $V_t=40$ cc.. This is consistent with the results from protocol #1. The overall effect of increasing the frequency from 2 to 5.5 Hz was to increase the base over apex ventilation ratio by about 9% around the mean value of 1.29 for a $V_t=80$ cc.. Similarly, an increase in frequency from 4 to 10 Hz at a $V_t=40$ cc. caused an average increase of 12% around a mean value of 1.135 in the *BASE/APEX* parameter.

The slope of the regression lines had a negative correlation with *FRC*. ($R = -.687$ for

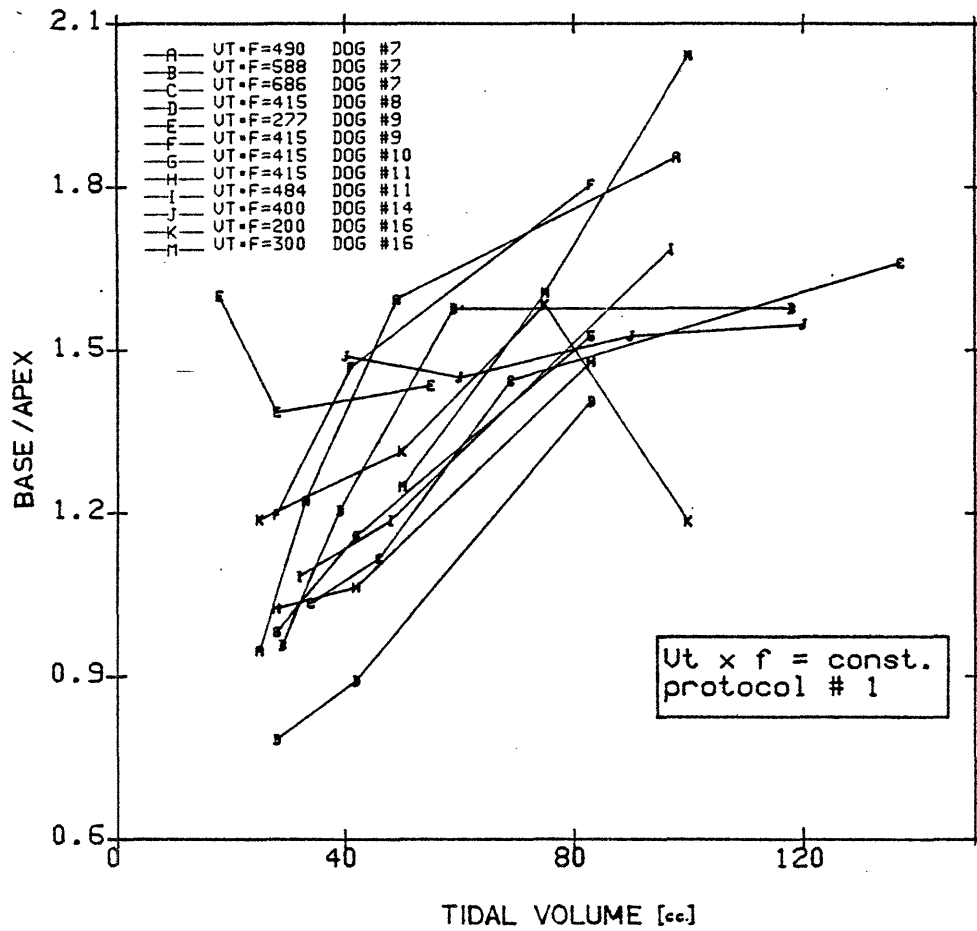


Figure 5-18:
 Experimental results from all runs in protocol #1 where E:I=1. Here, the ratio of the specific ventilation of the basal regions to that of the apical regions (BASE/APEX) is plotted against V_t for constant values of $(V_t \times f)$

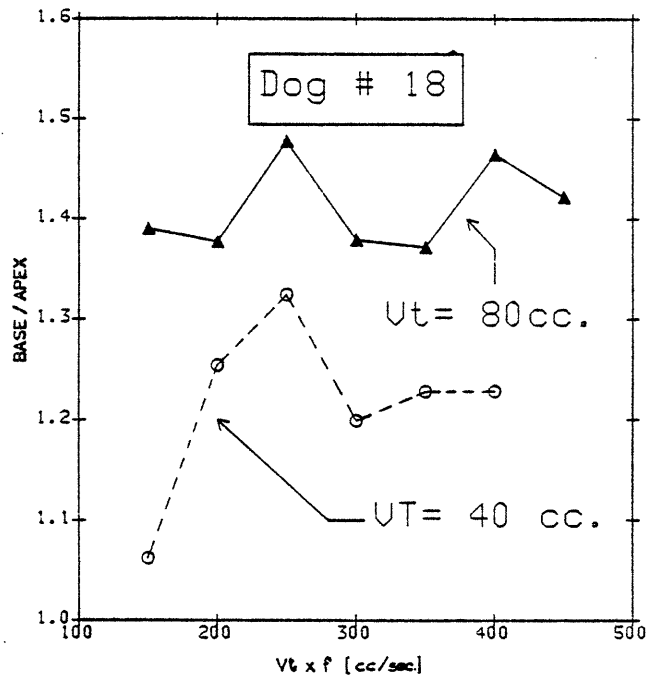


Figure 5-19:
 Typical plot of basal over apical specific ventilation vs ($V_t \times f$) for dog #18, protocol #2 where V_t was kept constant at 40cc. (circles) and at 80cc. (triangles)

$V_t=40$ cc. and $R = -.5877$ for $V_t=80$ cc.). This suggests that in the larger animals the increase in frequency minimally affected the distribution between apex and base, but in the smaller animals an increase in frequency increased preferentially the ventilation to the bases.

5.3 Summary of results in normal dogs

- Whole Lung Ventilation:

An expression for the specific ventilation of the whole lung ($SPVENT$) with HFV as a function of V_t/FRC and f was obtained from the data from 7 dogs. It was found that $SPVENT$ was approximately proportional to the square of the normalized tidal volume and to the first power of the frequency.

The Arterial $PaCO_2$ values during HFV correlated well ($R=.88$) with the total alveolar ventilation per kg. of body weight calculated from the ^{13}NN washouts. The value of total alveolar ventilation per kg. needed to maintain eucapnea with HFV was equal to 1.38 cc./sec.kg.. This value matched very well the value of alveolar ventilation per Kg. of eucapnic dogs at rest calculated from classical

pulmonary physiology expressions, namely 1.4 cc/sec.kg.

Finally, an expression that predicts the *HFV* ventilator settings needed to maintain eucapnea in dogs, given their weights and *FRC* volumes, was obtained.

- Regional Distribution of Ventilation:

The *MTT* visual images showed that, at the small tidal volumes, a region located medially near the base of the lungs, is ventilated at a higher rate than the rest of the lung. This region increased in size when the tidal volume was increased and the frequency decreased proportionally so that the $(V_t \times f)$ product was kept constant.

There was a modest but significant difference between the specific ventilation of the right and left lungs (up to 34%) which increased with V_t when $(V_t \times f)$ was kept constant. The increase in the whole lung ventilation produced by increasing V_t at constant $(V_t \times f)$ was directed mostly to the bases of the lungs, and so the *BASE/APEX* ventilation ratio increased with increasing tidal volumes to values up to 2.1. The histograms of specific ventilation generated from the *MTT* images showed that a bimodal distribution was present for the larger tidal volumes. The standard deviation of the histograms, corrected for measurement errors, (*SIGMA*), also increased with the tidal volume .

The effect of frequency at a constant tidal volume varied in direction and magnitude from dog to dog. However, it was found that the magnitude and direction of the frequency effect was correlated with the *FRC* lung volume of the animals. An increase of frequency, at a given tidal volume, decreased the right to left differences and the spread of the histograms for the larger animals but increased both of them for the smaller animals. The preferential ventilation to the bases was accentuated by the increase in frequency and the effect was generally stronger in the smaller animals.

5.4 Partially Occluded Airway

The results of this set of experiments are presented in table 5-II. The numbers on the table are the ratio of the specific ventilation from the unobstructed lobe to that of the obstructed lobe for the cases of balloon-inflated and -non-inflated, and for both *HFV* and *CV*. In EXP 1 and 3 the balloon obstructed the left lower lobe and in EXP 2 the right lower lobe.

It was found that for the balloon-inflated condition, the ventilation ratio between the unobstructed and obstructed regions was not significantly affected during *CV* (change in the

Table 5-II:

Summary of results from partially occluded airway experiments. The numbers on the table are the ratio of the specific ventilation of the unobstructed lobe to that of the obstructed lobe for the cases of balloon-inflated and non-inflated, for both *CV* and *HFV*

	BALLOON DEFLATED		BALLOON INFLATED	
	<i>CV</i>	<i>HFV</i>	<i>CV</i>	<i>HFV</i>
EXP #1	0.85	1.12	1.05	1.87
EXP #2	1.04	0.98	0.91	3.27
EXP #3	1.04	1.33	1.18	1.94
MEAN	0.97	1.14	1.05	2.34

ratio from .97 to 1.05), but was dramatically increased during *HFV* from 1.14 to 2.34.

Notice that the ratio of lobar *SPVENT*, for balloon deflated during *HFV*, is greater than unity for experiments #1 and #3, in which the *SPVENT* of the left lung was in the denominator. In contrast, the ratio was less than unity for exp #2 where the left lung *SPVENT* was in the numerator. This result is in agreement with the ones mentioned in the previous section since it means that during *HFV* for balloon-non-inflated, the right lower lobe was more ventilated than the left lower lobe.

Chapter 6

DISCUSSION

6.1 Total Lung Ventilation

CO₂ elimination in *HFV* has been studied recently by several groups ((Slutsky et al., 1980, Boun et al., 1980, Slutsky et al., 1981, Schmid et al., 1981, Fletcher and Epstein, 1982) and different mechanisms have been postulated as important.⁶ These mechanisms can be grouped into the following :

- *Augmented dispersion*: A coupling between longitudinal bulk flow and lateral mixing caused either by molecular diffusion or by secondary flows and eddies.
- *Streaming*: A net transport caused by a difference between the velocity profiles within the airways during inhalation and exhalation.
- *Pendelluft*: Where the frequencies used in *HFV* may be exciting inter-regional Pendelluft ventilation, thus 'alveolarising' the common bronchial spaces and decreasing the actual anatomic dead space.
- *Direct Alveolar Ventilation*: Lung inhomogeneities of several types (discussed in next paragraph), can result in a fraction of the tidal volume inhaled reaching the alveolar zone, thus participating directly in the gas exchange. Because a large $V_t \times f$ product is needed in *HFV* to maintain normocapnea (typically five to ten times the minute volume in *CV*), the fraction of tidal volume that needs to reach the alveolar compartment, or close to it, is only one-fifth to one-tenth of the tidal volume in order , to account for the total eucapnic ventilation. No direct experimental evidence, has been published to support this mechanism, although the findings of (Fletcher and Epstein, 1982), that showed a constant physiologic dead space at various V_t and f during *HFV*, seem to fit very well with this concept.

Independent of the mechanism of gas transport during *HFV*, the whole-lung ventilation results of this work agree very well with the experimental results from a timed averaged resistive model of bifurcations (Collins, 1982) in which the total volume flow of a tracer gas

⁶In Appendix B, a more detailed discussion of such mechanisms is presented.

(\dot{V}_{tr}) through a single bifurcation in oscillatory flow is expressed as:

$$\dot{V}_{tr} = A \times D_{eff} \times \frac{\partial C_{tr}}{\partial x} \quad (6.1)$$

where $(\partial C_{tr}/\partial x)$ is the spatial concentration gradient of the tracer gas and D_{eff} is defined as the effective diffusivity. The latter was found experimentally to be:

$$D_{eff} \sim \frac{u^{2.2}}{\omega^{1.3}} \quad (6.2)$$

where

$$u = \text{time average flow velocity}$$

and

$$\omega = 2\pi f$$

obtained for values of Reynolds (Rey) in the interval $(50 < \text{Re} < 700)$, and Womersley (α) in the interval $(4 < \alpha < 12)$

The above relation can be transformed, using an order of magnitude calculation, into an expression that can be compared with our experimental results. The flow velocity scales with:

$$u \sim \frac{(Vt \times f)}{L^2} \quad (6.3)$$

where 'L' is a characteristic length. Hence,

$$D_{eff} \sim \frac{Vt^{2.2} f^{0.9}}{L^{4.4}} \quad (6.4)$$

From the definition of D_{eff} (equation (6.1)), the CO_2 concentration gradient (ΔC_{CO_2}) across a bifurcation would scale with

$$\Delta C_{CO_2} \sim \frac{\dot{V}_{CO_2}}{D_{eff} \times L}$$

where \dot{V}_{CO_2} is the total volume flow of CO_2 through the bifurcation.

Since the CO_2 production of a dog at rest is related linearly with the body weight (BW) of the animal, substituting the expression for D_{eff} of eq.(6.4) the model would predict for a single generation that:

$$\Delta C_{CO_2} \sim \frac{BW \times L^{3.4}}{V_t^{2.2} \times f^{0.9}}$$

If we assume by geometrical similarity that $L \sim FRC^{1/3}$, then the same expression can be written as:

$$V_t^{2.2} \times f^{0.9} \sim \frac{BW \times FRC^{1.1}}{\Delta C_{CO_2}} \quad (6.5)$$

which, for a constant concentration gradient, is remarkably similar to expression (5.5).

Although expression (6.5) is only applicable to a single bifurcation over a limited range of α and Re_y , its similarity with (5.5), strongly suggests that the region limiting the CO_2 transport during *HFV* has similar transport characteristics to the above branching model.

Studies of short-term CO_2 elimination in dogs at the onset of *HFV*, however, do not give such close similarities. (Slutsky et al., 1981) found that the relation was of the form:

$$\dot{V}_{CO_2} \sim V_t^{1.49} \times f^{.92}$$

Of course, this regression equation is not meant for predicting the actual CO_2 elimination from the animals, since the data was normalized to arbitrary numbers and did not account for individual variations of lung volume and body weight. The formula only indicates the relative effects of frequency and tidal volume. (Slutsky et al., 1981) also found that in a

given dog the CO_2 elimination was not substantially affected by changes in *FRC*.

It should be said that the transport of ^{13}NN measured during a washout is not exactly equivalent to the transport of CO_2 measured during the first few seconds of *HFV*. On one hand, the molecular diffusivities for both gases are different and more importantly the CO_2 regional concentration existing at the start of *HFV* is a function of the regional distribution of the ventilation/perfusion ratios created during *CV*. Furthermore, the total rate of CO_2 eliminated is sensitive to regional inhomogeneities in blood flow while the specific ventilation measured from a ^{13}NN washout is not.

The following evidence, however, suggests that the expected differences between the two measurements should be small for healthy animals:

- It was found that the initial steep rise of an expirogram (Scheid et al., 1982), performed after a short period of washout with *HFV*, was identical for He and SF_6 . This finding strongly suggest that the transport of gases along the conducting airways is not greatly affected by the molecular diffusivity of the gas in question.
- The distribution of circulation in supine normal dogs is close to homogeneous and thus the elimination rate of CO_2 should not be dramatically different to the elimination rate of ^{13}NN .
- Furthermore, experimental results (Paloski et al., 1982) showed a strong correlation between the CO_2 elimination rate and the washout rate of Nitrogen in dogs. In addition, we found that the alveolar ventilation per kilogram needed to maintain eucapnea during *HFV*, using the ^{13}NN washout technique, agrees very well with values calculated from published data of basal metabolic production of CO_2 in dogs.

Besides the effect of the distribution of blood flow on the CO_2 elimination rate, several other reasons could also be responsible above-mentioned differences in the relative effect of V_t on the gas transport of CO_2 during *HFV*:

- In the system used in this study, fresh gas is introduced at the distal end of the endotracheal tube. In the configuration used by (Slutsky et al., 1981), however, the bias flow was located close to the proximal end of the endotracheal tube. It has been found more recently by (Gavriely et al., 1982) that the resistance to gas transport of the trachea and endotracheal tube can be as large as the resistance of the rest of the system. This finding is not surprising since this section of airway is primarily a straight tube, where the transport of CO_2 follows a different law. The

transport through a straight tube for $\alpha > 1$ and $(Rey/\alpha) > 200$ has been estimated (Kamm et al., 1982) as:

is of the form :

$$\Delta_{\text{TUBE}} C_{\text{CO}_2} \sim \frac{\dot{V}_{\text{CO}_2}}{Vt \times f} \quad (6.6)$$

Since from Eq.(5.5) the concentration gradient from the alveoli to the tip of the endotracheal tube, $(\Delta_{\text{LUNG}} C_{\text{CO}_2})$, approximately scales with

$$\Delta_{\text{LUNG}} C_{\text{CO}_2} \sim \frac{\dot{V}_{\text{CO}_2}}{Vt^2 \times f} \quad (6.7)$$

Then, the total concentration difference from the alveoli to a hypothetical bias flow $(\Delta_{\text{TOT}} C_{\text{CO}_2})$ as the one used in (Slutsky et al., 1981), can be estimated by adding (6.6) and (6.7):

$$\Delta_{\text{TOT}} C_{\text{CO}_2} \approx K_1 \frac{\dot{V}_{\text{CO}_2}}{Vt \times f} + K_2 \frac{\dot{V}_{\text{CO}_2}}{Vt^2 \times f} \quad (6.8)$$

where K_1 and K_2 are proportionality constants.

It does seem rather likely that for a constant CO_2 alveolar concentration, \dot{V}_{CO_2} could appear to have a dependency between the first and the second power of Vt when analyzed with a simple regression used by Slutsky et al. (1981).

- The flow waveform used in this study was square while the one used by (Slutsky et al., 1981) was sinusoidal. Until now, no study has been done to compare differences in the ventilation produced with these two waveforms. Thus this factor has to remain as one of the possible reasons for discrepancy until further measurements are performed.
- The findings of (Slutsky et al., 1981) concerning the effect of lung volume does not necessarily conflict with ours since they refer to the change in lung volume of a given animal and we are referring to a scaling factor from animal to animal. Since the volume of the central airways is not dramatically affected by changes in lung volume from a particular animal, large variations in the total lung alveolar ventilation are not expected with this maneuver. However, possible effects on ventilation due to changes in lung volume from a particular animal in Slutsky et al all experiments, might have been obscured by the fact that dead space of the apparatus was responsible for a large fraction of the resistance to the gas transport.

Since the efficiency of HFV with small tidal volumes is lower than that of CV, at tidal volumes greater than the dead space, it is clear that in order to ventilate a subject successfully with HFV, a much greater ($V_t \times f$) product is needed. This fact is of great significance when studying the regional distribution of ventilation during HFV because the relative importance of the different mechanisms of flow distribution is affected, among other things by the magnitude of the oscillatory flow rate ($V_t \times f$). Furthermore, the higher intra-bronchial flow rate needed for eucapnic HFV cause increased pressure drops along the airways. This can be partially responsible for the relative lack of effectiveness of HFV observed in patients with significantly elevated airway resistance, as it has been reported recently (Schuster et al., 1992).

More studies, however, are needed in the region of HFV where $V_t/V_d \sim 1$ and above which is the area where the most successful clinical applications have been reported (Sjostrand U., 1980, Klain and Smith, 1977, Bland et al., 1980, Turnbull et al., 1980, Carlon et al., 1982).

6.2 Distribution of ventilation

It appears that, to some extent, all the above-mentioned mechanisms might be acting during HFV. The actual contribution of each probably depends much on the actual parameters of HFV (V_t/FRC , α and Rey). For very small tidal volumes, augmented dispersion and streaming are the more plausible candidates while, for relatively larger tidal volumes, the contribution of the direct alveolar ventilation becomes probably the most significant. Whatever the actual mechanism may be, however, it is clear that the transport of the respiratory gases is directly coupled to the convective movement of gas within the airways. Thus the distribution of ventilation is directly related to the distribution of the oscillatory flows. This distribution is a complex phenomenon that can be affected

simultaneously by several mechanisms. From our results, however, it is impossible to identify with any certainty a particular mechanism. In the following paragraphs, several of the possible factors that could affect the distribution of ventilation during *HFV* will be presented without pretending more than a rough order of magnitude estimate.

6.2.1 Direct Alveolar Ventilation

Direct alveolar ventilation was presented earlier as a mechanism of gas transport. However, for obvious reasons, it is a cause of inhomogeneity in ventilation. Alveolar regions that are ventilated directly by fresh gas or that are located very close to the reach of the fresh air front will clearly be more ventilated than those where a more inefficient transport mechanism has to operate. Direct alveolar ventilation was certainly present during our experiments, for the tidal volumes close or larger than the estimated anatomical dead space. For tidal volumes smaller than the dead space, a modest deviation from an homogeneous regional distribution of flow rates could create a region of direct alveolar ventilation with a regional ventilation much greater than the rest of the lung.

Direct alveolar ventilation could hypothetically also exist in the presence of homogeneously distributed flow rates because of unequal bronchial pathway lengths. This possibility has been pointed out (Ross, 1957) based on direct measurements of plastic casts of dog bronchial trees. Accordingly, even at V_t smaller than the dead space, the alveoli located closer to the carina could receive some fresh gas, while those located farther away would receive mostly air already contained in the dead space. With the same argument, one would expect that, in a supine dog, the apical regions of the lungs would have a larger specific ventilation than the bases because the bronchial pathways are generally shorter to the apex than to the base. This hypothesis is in contradiction with our experimental findings which showed that for the larger tidal volumes (close to the anatomic dead space volume), the bases received a greater specific ventilation than the apex. Thus, one has to conclude that during

HFV, at the rates used in this study, the assumption of equally distributed flow rates is not valid.

6.2.2 Geometry of the Bifurcating Tree

The geometry of the bifurcating bronchial tree is one factor that could play a role in determining the distribution of flow in the lungs during *HFV*. As frequencies and flow rates are increased, the inertial forces become more significant and the angle of branching could become an important factor. In a single bifurcation, with equal cross-sectional area branches, the flow would prefer the straightest pathway.

The maximum pressure head difference that could result from a 180 deg angle from momentum consideration would be in the order of

$$\Delta P_{\max} \sim \rho u^2$$

Accordingly, for a typical dog under *HFV* at normocapnea with a $(Vt \times f) = 400$ [cc/sec], the value of ρu^2 in the main bronchi would be about 3.5mm. of H_2O . Although this is a relatively small number, compared with the total pressure amplitude with *HFV* at the same site (80mm. H_2O)⁷, this mechanism could play an important role in the distribution of alveolar ventilation when combined with the mechanism of direct alveolar ventilation for values of *Vt* approaching the dead space volume.

There are two additional ways in which the branching geometry could affect the distribution of ventilation during *HFV* which are illustrated in regions "I" and "II" of figure 6-1.

⁷These values have been calculated by (Akhavan R., 1983) for dogs using the (Horsfield and Cumming, 1978) model of the lungs and experimental results obtained from a model of rigid bifurcations.

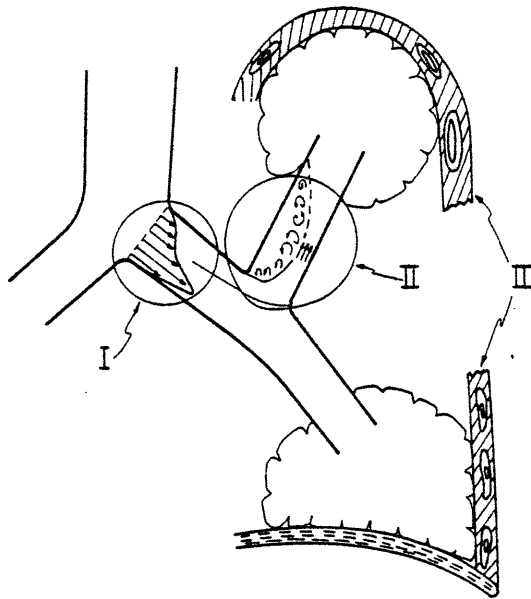


Figure 6-1:
Schematic of the central airways illustrating three possible causes of increased flow to the basal regions of the lungs. (For explanation see text)

Region "I" illustrates the shifting of the inspiratory velocity profile toward the medial wall of the main bronchus. In this way, the value of the dynamic head, $(1/2\rho u^2)$, of the flow within the stream lines directed to the basal bronchus can be greater than the dynamic head of the flow directed toward the apical bronchus. This effect was shown experimentally (Snyder et al., 1981) in a model of rigid bifurcations. Of course, the impedance to flow in the regions downstream of the branches would be competing with this partitioning effect.

Region "II" illustrates another plausible mechanism that could further decrease the flow to the apical region. Here, the jet like flow is created at the entrance of the apical bronchus because of the sharp change of direction. Since only a small portion of the dynamic head of the jet is recovered downstream in this type of flows, the pressure drop could be considerably

greater than the dynamic head calculated for a blunt velocity profile.

The meaning of region "III" will be explained in the following section.

6.2.3 Distribution of Dynamic Impedances

A further reason that could account for a nonhomogeneous distribution of flow rates during *HFV* is the distribution dynamic impedances within the lungs.

The air flow dynamics of the respiratory system can be represented approximately in a lumped parameter model as a network of resistances, inductances and capacitances in a branching configuration (Mead, 1961). There, the viscous pressure drops are modeled as resistive elements (R), the inertial pressure components as inductive elements (L) and the elastic compliance of the alveoli and bronchi, as capacitive elements (C).

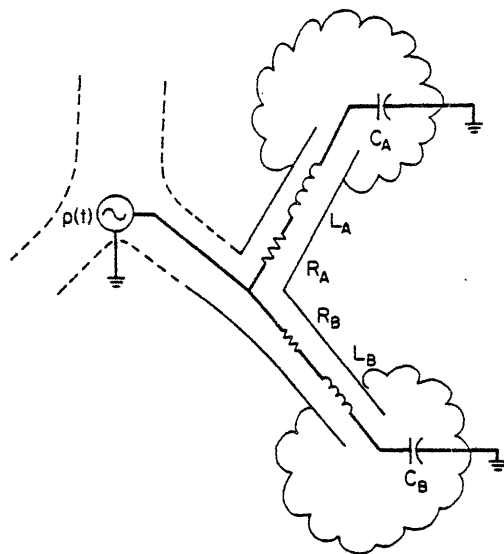


Figure 6-2:
Simplified electrical analog of
the flow distribution between the apex and the
base of a lung. For explanation see text

For the purpose of illustration, a simplified model of a single lung is presented in figure 6-2. Here $p(t)$ represents the pressure oscillations at the bifurcation of the main stem

bronchus, R_A , L_A and C_A represent respectively the resistance, inductance and compliance of the apical region and R_B , L_B and C_B represent the same parameters for the basal region. For simplicity the airway compliances have been ignored and the impedances of the trachea and main stem bronchus are not included. The equations for the network are

$$Q_A = \frac{p(t)}{R_A + [2\pi f L_A - (2\pi f C_A)^{-1}] \times j}$$

and

$$Q_B = \frac{p(t)}{R_B + [2\pi f L_B - (2\pi f C_B)^{-1}] \times j}$$

Assuming that the regional compliance of the lungs is distributed homogeneously, the capacitance of a region is then proportional to its volume and the total flow rate per unit volume, or specific flow (SPFLOW), is:

$$SPFLOW_A \sim \frac{Q_A}{C_A}$$

$$SPFLOW_B \sim \frac{Q_B}{C_B}$$

Thus, the regional distribution of flows between base and apex can be represented by the ratio

$$\frac{Q_B}{Q_A} = \frac{R_B + [2\pi f L_B - (2\pi f C_B)^{-1}] \times j}{R_A + [2\pi f L_A - (2\pi f C_A)^{-1}] \times j} \quad (6.9)$$

Notice that for low frequencies (as with *CV*) where $2\pi f \ll RC$ and $(2\pi f)^2 \ll LC$, the ratio becomes unity meaning that the distribution of flow is dominated by the distribution of the alveolar compliance, which we assumed proportional to the alveolar volume.

However, at large frequencies and large flow rates, as in *HFV*, the inductive and resistive elements may become an important factor in determining the distribution of the oscillatory flow.

Because the mathematical models of the tracheobronchial tree presently available assume symmetric branching, it is not possible to calculate the values of R_A , R_B , L_A and L_b in our

particular situation. Intuitively, however, one could expect that R_A and L_A should be smaller than R_B and L_B since the bronchial pathways to the basal alveoli are longer than those to the apical alveoli. Accordingly, equation (6.9) would predict apical regions would receive a larger flow rate per unit of lung volume than basal regions. This prediction is of course incompatible with our experimental findings. There is, nonetheless, some indirect evidence that the resistance of the shorter pathways could be greater than the resistance of the longer bronchial pathways under certain conditions. Ross (1957) calculated the pressure drop that would occur along different length pathways of dog bronchial casts. He assumed in his calculations, laminar flow and equal flow rate per terminal bronchus. It was found that the pressure drop was very similar along the shorter and the longer pathways. This remarkable result can only be explained if the geometry of the airways that he measured, was such that the velocity of the gas through the longest pathways, compared to the gas running through the shorter pathways, was lower in a proportion such as to compensate for the extra length that the gas had to travel. Although Ross' calculations might be valid for the low flow rates used during *CV*, they are certainly incorrect for *HFV*, where the high flows needed for eucapnea are no longer in the laminar regime. For example, at a $V_t=80\text{cc.}$ and $f=5\text{Hz.}$, it can be calculated that for the main bronchus, $(\text{Rey}/\alpha)\approx 420$. According to the experimental results for rigid bifurcations (Akhavan, 1982), the pressure drop along a given bifurcation follows a linear relation with the RMS flow for values of (Rey/α) less than 200 and a quadratic relation for values greater than 200. Thus, if the calculations by Ross were to be repeated using the quadratic relation in the pertinent regions of the tracheo-bronchial tree, the pressure drop along the longer pathways should be generally smaller than the one for the shorter. Furthermore, the assumption of equal flow per terminal bronchiole would no longer be valid and the specific flow along the longer pathways would be predicted to be greater than the specific flow along the shorter pathways.

The inductive pressure drops, on the other hand, are proportional to the length of the

pathway, and as Ross predicted, the longer pathways are expected to have a relatively larger inductive pressure drop than the short ones.

If the arguments from the last two paragraphs are proven to be true, the resistance to flow per unit of alveolar volume would be smaller for the bases than for the apex, but the inductance would have the opposite characteristics. This would be compatible with our findings from protocol #1 where, at a constant $V_t \times f$, the ventilation to the base increased when V_t was increased and f was proportionally decreased. In this case, by decreasing f , the inertial pressure drop to the bases would decrease while the frictional pressure drop remained constant. Furthermore, in protocol #2, the increase in frequency for a constant V_t would increase both the frictional and inertial pressure drops and the total effect on the distribution would depend on the relative magnitude of the frictional and inertial effects.

In the discussion of the preceding few paragraphs we have been assuming that the distribution flow rates is affected by the distribution of alveolar compliances through the lungs but we have not considered the effect of the chest wall. In normal breathing, the regional expansion of the lung parenchyma is relatively uncoupled from that of the chest-wall due to the sliding motion of the lubricated pleural surfaces (Brandi, 1972). Thus, in a supine dog at TLC, the degree of lung inflation along any horizontal plane is the same, even though the expansion of the thoracic cage at the base could be much greater than that at the apex. However, this uncoupling does not necessarily occur during *HFV* where the period of oscillation could be shorter than the time needed for the pleural sliding to occur. So in *HFV*, the relative inflation of the alveolar compartments might be more directly affected by the local chest-wall expansion. This mechanism, illustrated in "III" figure 6-1 could provide a further reason for the preferential ventilation to the base of the lungs during *HFV*.

The full test of these hypothesis, however, is out of the scope of this dissertation, and requires complex and detailed calculations based on actual anatomical measurements.

6.3 Gas Transport Distribution

Although the distribution of flow rates is of major importance in determining the distribution of alveolar ventilation, it is useful to contemplate another fact related to the transport mechanism that can affect the resulting distribution of the effective ventilation.

6.3.1 Interregional Mixing

Interregional mixing can occur because of Pendelluft, under very special conditions of resonance, and also because the presence of a common dead space that acts as a mixing chamber for the compartments served by its branches. A common dead space has the effect of transporting gases from the region of higher concentration to those of smaller concentration and tends to make more homogeneous the concentration of intrapulmonary gases. Consequently, during a wash-out maneuver in the presence of different flow rates to two hypothetical compartments, the more ventilated of the two could only decrease its concentration to the level which the common deadspace is allowed to reach by the slower compartment.

6.4 Previous Work

(Schmid et al., 1981), using six collimated scintillation detectors, studied the regional distribution of ^{133}Xe clearance rates by *HFV* with one tidal volume and two frequencies. The regional distribution and subsequent clearance of ^{133}Xe after a right atrial bolus injection was also studied. A small but significant difference was found in the clearance rates from the base and the apex. Also, a small decrease was observed towards unity in the base-to-apex ventilation ratio after an increase in frequency from 15 Hz to 30 Hz.

Although qualitatively those findings are similar to the ones reported here, several differences in methodology distinguish their work from ours and can explain the discrepancies

in the magnitude of the trends observed.

- The location of the bias flow was proximal from the endotracheal tube. It has been recently shown that the endotracheal tube can account for a resistance to gas transport as large as the total animal resistance (Gavriely et al., 1982). Furthermore, the bias flow rate was only 10 l/min for oscillatory flow rates of 45 l/min. From the mean clearance rate and lung volume measurements reported, the concentration of ^{133}Xe at the bias can be estimated as about 20% of the alveolar concentration. Both of the above-mentioned facts tend to create a more homogeneous ventilatory pattern due to the interregional mixing occurring in the apparatus deadspace and to the rebreathing of ^{133}Xe .
- The *HFV* apparatus used a motor driven piston to generate the oscillatory flow. According to their description, they had a chamber between the piston pump and the endotracheal tube. Because of large changes in the impedance of the endotracheal tube and the animal, as the frequency was increased, it is very likely that at 30 Hz an appreciable fraction of the piston displaced volume was lost due to the compressibility of the air. In our system, the total delivered tidal volume is independent of the animal's dynamic impedance and its composition is totally independent of the ventilator settings.
- The clearance rates were calculated by fitting a monoexponential function to the data corrected for the "thoracic walls" clearance rate, since the ^{133}Xe is soluble in body tissues and in blood. By subtracting the "background" with a "by eye" method, any regions with clearance rates slower than $.003\text{sec}^{-1}$ were automatically eliminated.
- The relatively low energy gamma rays of ^{133}Xe are sensitive to attenuation when they travel through body tissues; thus, the measurements with the detectors are more sensitive to emissions originating near the pleura than those from the more internal regions.

A different approach for the measurement of the \dot{V}/Q inequality was used in the experiments described below.

Two groups, (Robertson et al., 1982, McEvoy et al., 1982), used the multiple inert gas technique⁸ to study the distribution of ventilation perfusion ratios during *HFV* and compare it with *CV*. Although the use of a 50 parallel compartment model to explain the data is inadequate, the raw data show an enhancement of the elimination of the most soluble inert gases. This fact is compatible with a major degree of ventilation-perfusion inequality where

⁸described in appendix A.4

about half of the alveolar ventilation is distributed to lung units of \dot{V}/Q ratios > 20 . This gross maldistribution was attributed primarily to a methodology artifact by which the most soluble gases transport was enhanced by the interaction of the convective gas flow and diffusion between the gas and the liquid lining of the airways (McEvoy et al., 1982). It was shown in a model that the presence of a liquid in the surface of the airway in fact increased the amount of transport.

Although this may explain part of the disproportionate maldistribution, it does not exclude the possibility of a more moderate but still significant degree of inhomogeneity in the distribution of ventilation during *HFV*.

From our results, the magnitude of the specific ventilation of a hyperventilated region can be estimated by assuming that its volume is a fraction (h) of the total *FRC* volume. Since the volume of the basal regions was in average about 70% of the lung volume⁹, the Apex/Base specific ventilation ratio would be :

$$\frac{BASE}{APEX} = \frac{h \times SPVENT_f + (0.7 - h) \times SPVENT_s}{0.7 \times SPVENT_s} \quad (6.10)$$

where $SPVENT_f$ = the specific ventilation of the hyperventilated region and $SPVENT_s$ = the specific ventilation of the rest of the lung. From this, the ratio of the specific ventilation of the hyperventilated region to that of the rest of the lung can be expressed as

$$\frac{SPVENT_f}{SPVENT_s} = \left(\frac{BASE}{APEX} - 1 \right) (0.7/h) + 1 \quad (6.11)$$

where $BASE/APEX$ is the ratio between the specific ventilation of the apex to that of the base.

The fraction of the total ventilation going to the hyperventilated compartment could be

⁹Calculated from the equilibrated images

estimated as

$$\frac{VENT_f}{VENT_{tot}} = \frac{SPVENT_f \times h}{(SVENT_f \times h) + SVENT_s \times (h-1)}$$

So, for an extreme case, where Base/Apex=2.3 and assuming $h=.2$, the hyperventilated region would be ventilated at a rate 5.6 times the ventilation of the rest of the lung. For the same case the fraction of the total ventilation used in the fast compartment would have been about 58 % of the total ventilation. This is a more moderate inhomogeneity than the ones reported by McEvoy et al. (1982).

6.5 Cross-sectional Area

The importance of the geometry of the large airways in the distribution of ventilation during *HFV* is further stressed by the results of the experiments where partial occlusion of a bronchus was artificially created.

This observation suggests the possibility of using the radioactive gas washout study in conjunction with the *HFV* technique as a non-invasive method of detecting airway obstruction at stages where a normal $^{13}N_2$ washout study alone would not be sensitive enough to detect it. A detailed description of the method is found in Appendix E.

Chapter 7

CONCLUSIONS

The High Frequency Ventilator that we developed can generate precise tidal volumes (20cc to 150cc) at frequencies from 1 to 25 Hz with a square flow rate wave form and a variable E:I ratio (1:1 to 1:5). This ventilator has the unique feature of delivering tidal volumes independent of the animal lung impedance.

A relationship was established that can predict what settings of the respirator are needed during HFV to produce eucapnea in dogs of different lung volumes and weights.

From our results we conclude that the FRC volume is a very important normalizing, in the sense that V_t/FRC rather than V_t alone correlates the results from different animals.

The relative effects of V_t and f on the overall gas transport was of the form:

$$\left(\frac{SPVENT}{f}\right) = 4.25 \left(\frac{V_t}{FRC}\right)^{1.99 \pm .14} \left(\frac{FRC^{2/3} f}{\nu}\right)^{-0.14 \pm .12}$$

We conclude that the individual effect of the Womersley parameter ($\alpha \sim (FRC^{2/3} f / \nu)^{1/2}$) on the overall lung Specific Ventilation is small and not significant. Ignoring α from the regression, the resulting expression can be written as:

$$SPVENT \approx 1.9 \left(\frac{V_t}{FRC}\right)^{2.1 \pm .10} \times f$$

We found that the regional distribution of ventilation was, for a constant ($V_t \times f$), more homogeneous at smaller tidal volumes and higher frequencies than it was at larger tidal volumes but smaller frequencies. The overall ventilation of the lung, in contrast, was enhanced with larger tidal volumes.

Our result showed that the bases of the lung are ventilated more than the apex with differences as high as 100 %. These large differences prove that the distribution of flow

rates is not homogeneous during *HFV* and suggest that the mechanism of direct alveolar ventilation may play a major role at tidal volumes of the magnitude used in this study.

This pattern of preferential basal ventilation can be attributed to a combination of direct alveolar ventilation with one of several factors such as non-homogeneous distribution of dynamic impedances, differences in the angle of branching of the bifurcations, and the flow partitioning effect of a system of bifurcations in cascade. Our data, however, do not provide enough information to allow calculations of their relative contributions.

The distribution of ventilation during *HFV* was much more affected by a partial airway obstruction than during *CV*. This last finding suggests the interesting possibility for using the technique, developed in this thesis work, as a non-invasive method of detecting obstructions of the large bronchi.

Appendix A

PULMONARY VENTILATION

This appendix is written for those readers not familiar with respiratory physiology. It includes an overview of the pertinent physiology of normal and artificial ventilation. The relevance of the regional distribution of ventilation is presented, and the different methods used for its quantification are discussed.

A.1 Physiology of Normal Respiration

The primary function of the respiratory apparatus in mammals is to allow oxygen to move from the air to the blood and to allow carbon dioxide to move out. Gas is brought to one side of the blood-gas interface by airways and blood to the other side by blood vessels.

The airways consist of a series of branching tubes which become narrower, shorter and more numerous as they penetrate deeper into the lung. There are about 19 generations of conducting airways, where the trachea is the largest and the terminal bronchioles the smallest airways without alveoli. This set of airways is called the *anatomical dead space* since they merely conduct the air in and out of the alveolar zone where the actual gas exchange between blood and air takes place.

The respiratory or alveolar zone is made up of respiratory bronchioles, alveolar ducts and alveoli. The distance from the terminal bronchiole to the most distal alveolus is only about 5 mm but the respiratory zone makes up about 90 % of the lung volume. For one of the typical dogs used in this study with a resting lung volume of 1 liter, the anatomical dead space at *FRC* is about 80 cc.

During inspiration, the volume of the thorax increases and air flows into the lung.

Inspired air travels as bulk flow to approximately the level of the terminal bronchioles. Beyond this point, because of the large total cross-sectional area, molecular diffusion takes over as the dominant mechanism of ventilation in the respiratory zone.

Exhalation is produced passively by the elastic recoil of the combined lung-thorax structure and the lungs return to their pre-inspiratory volume called *Functional Residual Capacity* or '*FRC*'.

The pulmonary blood vessels also form a branching network from the pulmonary artery through the capillaries to the pulmonary veins. The capillaries form a fine net in the walls of the alveoli where blood and alveolar gas are only separated by a thin membrane of less than 0.5 microns thickness.

A.2 Artificial Ventilation

Patients under general anaesthesia or those suffering from certain diseases have to be artificially ventilated . This is normally done using a ventilator that forces the air or respiratory gases into the lungs of the patient. In conventional ventilation (*CV*) the volume of air that is introduced to the lungs at each breath (Tidal volume) is much greater than the volume of the conducting airways and a large fraction of the fresh air inhaled reaches the respiratory zone. In this case, the Alveolar Ventilation (\dot{V}_{alv}), which defines the total volume of fresh gas ventilating the alveoli per unit time, can be calculated as:

$$\dot{V}_{alv} = (Vt - Vd) \times f \quad (A.1)$$

where

Vd = Anatomic dead space volume
 Vt = Tidal volume
 f = Frequency of ventilation.

The first type of respirators used, created a negative pressure around the body which

was confined in a sealed box that left only the head outside. This method attempted to imitate the normal physiology of the respiratory system by providing normal tidal volumes and normal intrathoracic pressures (around atmospheric pressure) to the patient. There were, however, several inconveniences in terms of patient management, and the method did not provide enough ventilation under certain pathological conditions.

The most common artificial ventilation system used at present is called 'Intermittent Positive Pressure Ventilation' (IPPV). This method forces air into the lungs of the patient through an endotracheal tube. The pressures generated in the thorax are higher than the physiological ones but, when applied to normal, healthy individuals, they do not produce noticeable side effects. However, in diseases where the lung compliance is decreased, as in pulmonary edema, extremely large pressures are needed, resulting in barotrauma to the lung parenchyma and impairment of cardiac function.

Furthermore, in cases of air leaks, as in a bronchopleural fistula, most of the delivered tidal volume is lost through the leak, making it impossible to maintain adequate alveolar ventilation during *CV*.

A.3 Distribution of Ventilation

(Physiological Significance)

Ideally, the ventilation distribution should match the circulation distribution so that all the blood is exposed to alveolar gas of the same composition. Unfortunately, mismatching of ventilation and blood flow within various regions of the lungs is present even in normal conditions. Alveolar zones which are poorly ventilated but well perfused have concentrations of CO_2 and O_2 very close to the mixed venous concentration and the gas exchange is inefficient. In the other extreme, ventilation to poorly perfused-regions can, for practical purposes, be considered as waste.

Several causes of mismatching, indicated by variations in the ventilation-perfusion, (\dot{V}/Q), have been recognized:

- In normal lungs
 - * Gravity effects on blood distribution
 - * Gravity effects on lung inflation.
- In pathological cases
 - * Airway obstruction
 - * Parenchymal disease
 - * Pulmonary embolism
 - * Tumors.

The physiologic consequences of \dot{V}/Q mismatching are poor oxygenation and if the matching is severe enough CO_2 retention that can not be improved by increasing the total ventilation.

A.4 Measurement of Distribution of Ventilation

- MULTIPLE GAS DILUTION

Six inert gases (sulfur hexafluoride, ethane cyclopropane, enflurane, diethyl ether, and acetone) are dissolved in isotonic saline and infused into the saphenous vein at a constant rate. After 30 minutes of equilibration time, pulmonary artery and femoral artery blood and mixed expired gas samples are drawn. The inert gas concentrations in each sample are measured and retention ratio (R) (defined as the ratio of arterial to mixed venous partial pressures), and excretion (E) ratio (defined as arterial to exhaled gas partial pressures), are calculated. The data are then plotted against blood-gas partitioning coefficient to obtain R-E solubility curves. The distributions of ventilation and blood flow are then calculated for a 50 compartment lung model with parallel inequality consistent with the pattern of inert gas data (Wagner et al., 1974)

Although the mathematical validity of the solution for the 50 compartment model has not been established, this method provides a tool to assess in a semi-quantitative manner the distribution of the ventilation/perfusion ratio. The

method however, does not differentiate between hyperventilated areas and hypoperfused ones.

- TOTAL LUNG WASHOUT OF A TRACER GAS

This method consists of rebreathing gas labeled with a tracer until it is distributed homogeneously throughout the lungs and then breathing from a tracer-free gas while monitoring the concentration of the expired gases. The tracer gas has to be very insoluble in the blood and tissues in order to limit the measurement to the lung air spaces.

The recorded signal of tracer gas elimination rate vs time, is fitted with a multiexponential function and the system is then modeled as a multicompartamental parallel system. Each hypothetical compartment is characterized by a fractional volume and a washout time constant. The disadvantage of this system is the arbitrary assumption of a parallel compartment model which is not necessarily related to reality. Also, the fitting algorithm is generally a source of errors.

- V/Q SCANS WITH RADIOACTIVE TRACERS

Blood flow is generally assessed by imaging the lungs after an intravenous bolus injection of solution of a gas which is highly soluble in air but poorly in blood, during breath-holding at total lung capacity. Since the majority of the gas diffuses into the airspaces, the distribution of activity within the lungs represents the distribution of the regional blood flow.

Ventilation can be estimated by imaging the lungs, during breath holding at TLC, after a single breath of a gas containing a radioactive tracer. A disadvantage of this method is that it does not provide a reference lung volume and makes it difficult to interpret the test results.

Ventilation can also be measured regionally by imaging the lungs during a washout maneuver after a period of equilibration with the radioactive tracer. This method is the one used in this study and is described in the main text.

The disadvantage of imaging methods, in general, is that they only provide a coarse spatial resolution which is not enough to detect intra-regional inhomogeneities. However, they have been extremely useful in the detection of inhomogeneities of larger topographical regions and are currently being used in the clinical setting.

Appendix B

MECHANISM OF *HFV*

Because the classical physiology concept of ventilation, summarized by equation (A.1) is not valid for *HFV*, several mechanisms have been postulated to explain the mechanism of gas transport during this method of ventilation. In this appendix a quick overview of the most commonly accepted mechanisms is presented. A more detailed review can be found in (Kamm et al., 1982).

B.1 Augmented Dispersion

This mechanism results from the interaction between axial bulk flow and radial dispersion (Taylor, 1954).

In the case of laminar flow in a straight tube, axial transport of a tracer, \dot{V}_{tr} , is primarily due to molecular diffusion. This transport mechanism was studied analytically for a sinusoidal flow waveform by (Chatwin, 1975) and (Watson, 1982) and confirmed experimentally by (Joshi et al., 1982). Their results can be expressed in the form:

$$\dot{V}_{tr} = A \times D_{eff} \times \frac{\partial C_{tr}}{\partial x} \quad (B.1)$$

where D_{eff} is defined as an effective longitudinal diffusivity given by:

$$D_{eff} = D_{mol} + F(\alpha) (a \times u_{rms})^2 / D_{mol} \quad (B.2)$$

where α = womersley parameter, a = tube diameter and u_{rms} = root-mean-square value of the cross-sectional average velocity. $F(\alpha)$ is a function that ranges from a constant value of 1/48 for $\alpha < 1$ to $(2\sqrt{2}\alpha^3)^{-1}$ for $\alpha \gg 1$.

In the case of turbulent flow or when the geometry of the system is such that

secondary flows are generated in a complex velocity field, the molecular diffusivity is replaced by a turbulent diffusivity (Kamm et al., 1982).

B.2 Streaming due to Asymmetric Velocity Profiles

It has been shown experimentally that as a result of the difference in the time-averaged velocity profiles during inhalation and exhalation, a net amount of mass transport results after each oscillatory cycle (Haselton and Scherer, 1980). The net mass flux across any plane would be :

$$V_{tr} = Q_{bd} \frac{\partial C_{tr}}{\partial x}$$

where Q_{bd} is the bi-directional flow rate and $[\partial C_{tr}/\partial x]$ is the spatial concentration gradient. Notice that this expression can be interpreted as a diffusive-like mechanism in which the transport is proportional to the local concentration gradient even though molecular diffusion is not playing any role.

B.3 Pendelluft

The oscillatory flow dynamics of the respiratory system can be modeled as a branching system of lumped parameters (Mead, 1961). In normal lungs under *CV*, the ventilation of all alveoli occurs synchronously and its relative magnitude is determined primarily by the alveolar compliance properties. The situation may become different when the frequency is increased as in *HFV*. Under those conditions, the alveolar ventilation could become so asynchronous that some of the alveolar compartments might be still inhaling while the others are already exhaling. Therefore, some of the alveoli could be receiving alveolar instead of fresh gas.

The rebreathing of alveolar gas by this mechanism tends to make the alveolar spaces and the common dead spaces more homogeneous and therefore decreases the effective

deadspace volume.

Experimental studies, using high speed photography (Lehr , 1981), have shown that different areas of the pleural surface of excised lungs move out of phase with each other during *HFV*. This suggests that interregional bulk gas flow may be present. However, the extent to which this mechanism is acting in a physiological situation is not yet defined where the lung surfaces are constrained by the thoracic walls. In fact, it is unclear as to whether the observed movements are only surface deformations without a real interregional volume transfer.

So far no theoretical models have been developed that can predict quantitatively the effect of this mechanism on the overall pulmonary gas transport.

B.4 Direct Alveolar Ventilation.

Direct alveolar ventilation occurs when part of the inspired tidal volume reaches the alveolar compartment and has the same characteristics of conventional ventilation. Although this mechanism may not play any role in *HFV* for tidal volumes much smaller than the anatomical dead space, it is very likely that it plays a major role in *HFV* for tidal volumes above one-half of the dead space. Several reasons can account for the fact that some fraction of the inspired gas could reach part of the alveolar region at tidal volumes smaller than the dead space:

- First, because of the complex geometry of the bronchial tree the velocity profiles are not blunt , even at relatively high Womersley numbers. Consequently, the penetration distance of a fraction of the inspired gas front can be considerably longer than that predicted by a blunt velocity profile. (For a hypothetical parabolic profile, assuming no lateral diffusion, the penetration distance is twice as long as that for a blunt profile.)
- Second, because of lung inhomogeneities, there are pathways to alveoli that have smaller dynamic impedance to flow than others and, thus, the front of inspired gas will reach those alveolar regions first.

- Third, the momentum of the inspired flow makes it more likely for the flow to follow the straightest pathways reaching the alveoli that are located downstream from such pathways first.

- Fourth, even in the case where fresh inspired gas does not reach actual alveolar compartments, it may reach areas very near to the well-mixed alveolarized zone. In this case, the resistance to gas transport becomes very small and those regions are ventilated as if they were directly ventilated.

Appendix C

THE HIGH FREQUENCY VENTILATOR

C.1 Description

The schematic of the *HFV* system, presented in figure 2-1 page 15, is described in more detail in the following paragraphs.

A flow of oxygen at 50 psi was measured with a rotameter before it was regulated with a choked flow needle valve to produce a constant flow rate independent of the downstream pressure. The respiratory gas then entered a 2 gallon tank that served as capacitance. At the exit from the tank, the flow was chopped by a variable speed rotary valve and introduced to the animal via a regular endotracheal tube. Different rotary valves with close-to-open duty cycles of 1:1, 2:1 and 4:1 could be mounted on the system.

A specially modified vacuum regulator, feed-back controlled by the mean airway pressure signal, maintained a steady suction flow through a high impedance expiratory tube of 2mm ID and 30cm length from the animal.

FIGURE 2-2, page 15, shows the configuration of the tubes connecting the ventilator to the animal. A 10 mm. ID endotracheal tube was used and the expiratory tube entrance was located about 1 cm. proximal to the tip of the endotracheal tube.

Mean airway pressure was measured through a 1 mm. ID catheter located 15 cm away from the tip of the endotracheal tube, at the level of the main stem bronchi.

Inhalation occurred while the rotary valve was opened and fresh gas, at a constant flow rate, was injected through the endotracheal tube. During this period, a fraction of this flow was being simultaneously removed by the expiratory line. When the rotary valve closed,

inspiratory flow stopped abruptly and the expiratory tube continued to extract gas at the same constant rate, thus starting the exhalation period of the cycle.

The delivered tidal volume can be calculated from the frequency f , the total flow (Q) and valve duty cycle. Figure C-1 shows a hypothetical flow wave form delivered by the rotary valve to the animal (\dot{V}_{in}) and the wave form of the extracted gas (\dot{V}_{out}). From conservation of mass it follows that:

$$\dot{V}_{out} = Q$$

and

$$\dot{V}_{in} (I) = Q (E + I)$$

$$(\dot{V}_{in} - Q)I = Vt$$

Thus, the tidal volume (shaded area) is,

$$Vt = Q \times E$$

Further,

$$f = \frac{1}{E+I}$$

Hence

$$Vt = \frac{Q}{f} \times \frac{E}{E + I} \tag{C.1}$$

The time constant of the combination of tank-valve and conducting system ($>10\text{sec}$) was designed to be much longer than the period of the oscillations during *HFV*. Thus, the system behaved as a constant flow source and the wave form of the delivered flow was remarkably close to a square wave. This is clearly shown in figure 2-3, page 16, where traces of the volume waveform vs time are shown, as measured from the pressure excursions

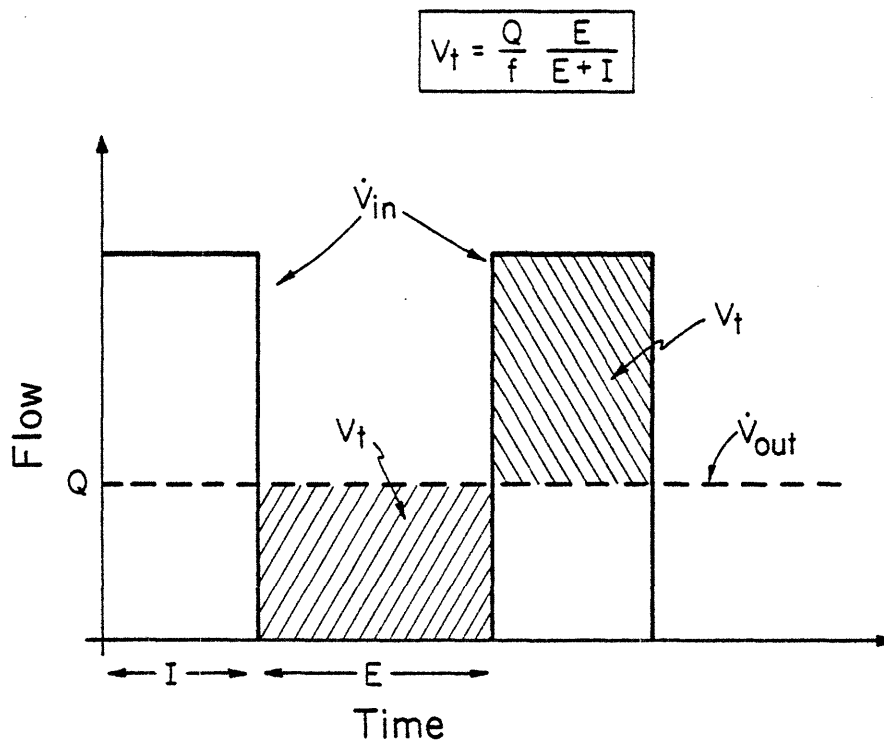


Figure C-1:

Plot of Flow vs time illustrating the way to calculate the tidal volume (V_t) delivered by the HFV device. \dot{V}_{in} = volume entering the system through the rotary valve. \dot{V}_{out} = volume leaving the system by the high impedance suction duct.

produced on a calibration tank by the HFV device. Both curves were obtained with the same gas flow through the device and with the same E:I ratio valve, thus have the same oscillatory flow characterized by the product ($V_t \times f$). The trace on the left corresponds to a $V_t = 80$ cc. and a $f = 5$ Hz., and the one on the right to a $V_t = 40$ cc. and a $f = 10$ Hz.

C.2 Calibration Tests

Equation (C.1) was validated experimentally measuring the pressure oscillations produced in a calibration tank into which was introduced rapidly a known volume of gas. Because the thermal time constant of the tank ($\tau > 10$ sec.) was larger than the period of oscillation during HFV, the process could be considered adiabatic during the volume calibration.

Figure C-2 presents the results of the calibrations. The X axis is the calculated $V_{t_{cal}}$

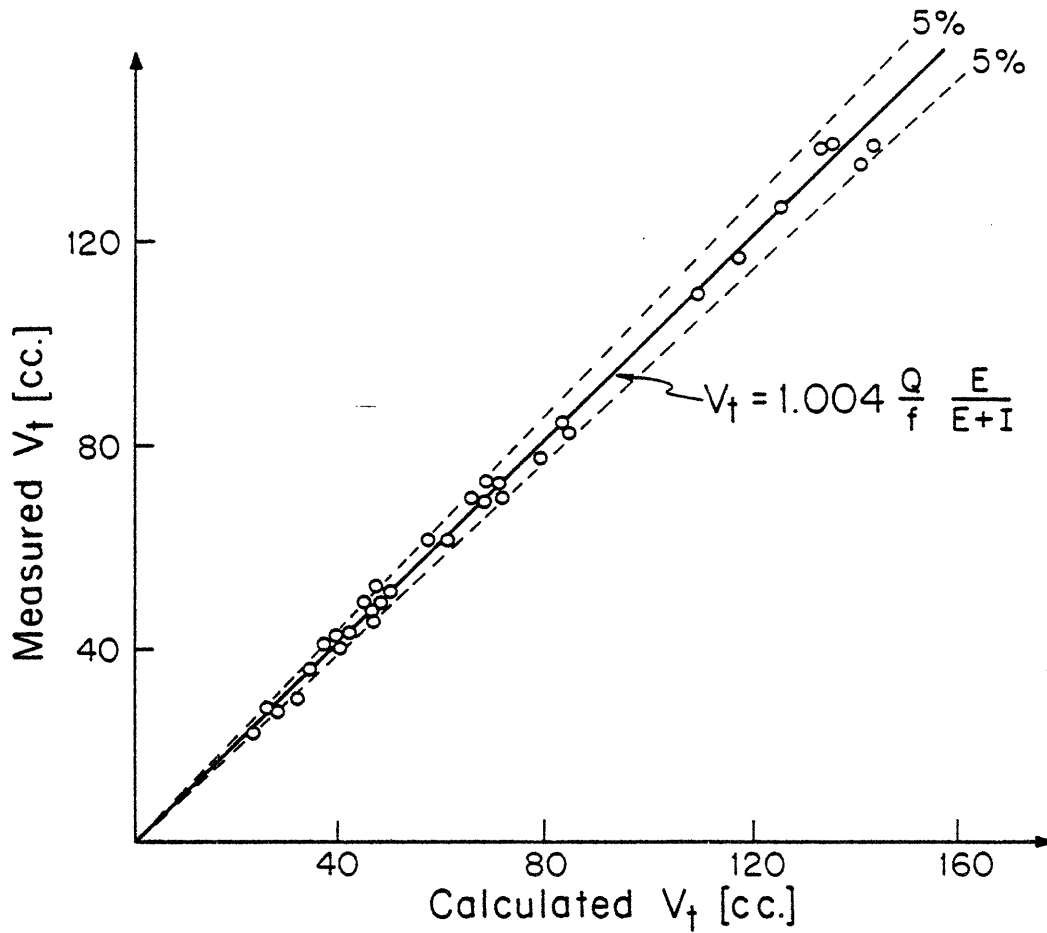


Figure C-2:
 Calibration graph for the V_t delivered by the HFV device. The 'X' axis is the calculated value of V_t in cubic cm.. The 'Y' axis is the measured value of V_t from the recorded pressure signal generated on a calibration tank by the HFV device

from equation (C.1). The equation of the best fit line is:

$$V_{t_{\text{meas}}} = (1.004 \pm 0.037) \frac{Q}{(1 + I/E)} \quad (\text{C.2})$$

with correlation coefficient $R^2 = .99$

Because the flow is choked at the needle valve, the delivered tidal volumes are independent of changes in the animal's dynamic impedance. This characteristic was verified by repeating the calibration with a tank of a smaller volume and finding that the delivered tidal volume was unchanged.

C.3 Characteristics and Advantages

This *HFV* system can generate precise tidal volumes with clean square waveforms, allowing for accurate and independent control of:

- Oscillatory flow, characterized by the product of $V_t z f$, by changing the flow regulator setting;
- The ratio of the expiratory time to the inspiratory time and the frequency of ventilation by changing to a rotary valve of a different duty-cycle and by varying its rotation velocity respectively;
- The mean airway pressure and *FRC* by changing the vacuum regulator setting.

In contrast to most of the *HFV* systems described in the literature, in our system the total inspired volume is made of 100% fresh gas with essentially no contamination from the exhaled gases.

Appendix D

MEASUREMENT ACCURACY

In this appendix, the positron camera is described and the statistical implications of the data manipulation as well as the corrections used on the data are discussed.

D.1 The Positron Camera

This camera was designed and developed at the Massachusetts General Hospital (Brownell and Burnham, 1974). In the following paragraphs a short description of the camera and the cinematographic data processing method will be presented. A more detailed description can be found elsewhere (Pizer et al., 1974, Brownell, Correia and Zamernhof, 1977).

The principle of positron imaging is based on the physical process that positrons undergo following their emission by a beta-unstable radioisotope. After emission, the positron follows a ionization path through the material in which it is emitted. After the positron slows down, it combines with a valence electron and the system undergoes the process of annihilation with the creation of two photons. In order to conserve energy and momentum the two photons are emitted in opposite directions at an angle of $180^\circ \pm .03^\circ$.

The positron camera consists of a pair of two-dimensional arrays of detectors that are parallel and facing each other. The system is designed to register an event only when two directly opposite detectors record the annihilation of photons simultaneously. Whenever an annihilation event is detected in coincidence by the two detectors, the event is assumed to have originated somewhere along a line joining the detector centers.

A positron imaging system has at least two major advantages over a conventional photon imaging system such as a gamma camera. First, since the positron system requires no

physical collimation to achieve spatial resolution, sensitivity is greatly increased. Second, since the production of a true coincidence count requires that both photons escape unscattered from the section of the body being imaged, the positron image system, unlike the conventional photon imaging system, is isosensitive to positrons emitted along a coincidence line through the body. The possibility of random coincidence detections is a potential source of error in the measurement but it is negligible for count rates of less than 1000 counts/second.

Because the occurrence of the radioactive decay events follows a Poisson process distribution, the expected standard deviation of a measurement is equal to the square root of the number of events registered. Since the initial total count rate used in the experiments was about 1000 count/sec distributed over 600 pixels, the expected relative error of the raw data per pixel for a 10 seconds collection is:

$$\begin{aligned} \text{relative error} &= (1/\sqrt{N}) \\ &= 1/\sqrt{1000 \times 10/600} \\ &\approx .25 \end{aligned}$$

In order to improve the statistical certainty of the measurement, the raw data were subjected to a smoothing function. This operation is a built-in feature of the system used. It consists of assigning to a pixel the sum of one-half of its value and one-fourth of the value of each of its four neighboring points. By using this procedure, the expected value of the relative error is reduced to 44% of its original value. When the operation is performed a second time, the expected relative error is further reduced to 24.4%. These reductions of error are obtained at the expense of resolution and so, it is desirable to minimize their use. In order to decide the number of smoothings to perform, a sample set of experiments was analyzed using the smoothing function on the raw data once, twice and four times, respectively. It was found that as the number of smoothings increased, the standard

deviation of both the error histogram and the specific ventilation histogram decreased. The greatest difference between these two values (and thus the better signal-to-noise ratio) was found with two smoothing operations.

The positron camera was controlled by a computer operational system, known as (PLS), that allows for mass storage of and further processing of the data. The operational system corrects automatically for the tracer decay time constant, allows for the definition of "areas of interest," generates visual images and performs several mathematical manipulations on the collected data.

D.2 Mean Transit Time Image

An image proportional to the regional *MTT* was obtained by dividing, for each pixel, the sum of all images collected during a washout maneuver by the corresponding image collected during equilibration for that particular run. After this operation, the expected relative error of the resulting image can be calculated to be the square root of the sum of the squares of the relative errors of the two images involved in the division.

In order to further improve the statistical certainty the sum of all the equilibration images, collected for the same dog, was used instead of that corresponding to each run. The following paragraphs analyze the statistical implications of the above operation.

Let $c_e(i,k)$ be the number of counts in pixel (i) of the equilibrated image of run k ($\approx c_e$, since all runs had about the same initial count rate).

The number of counts in pixel "i" of the sum of all "k" equilibration images ($c_s(i)$) will then be:

$$c_s(i) = \sum_k c_e(i,k) \approx k c_e$$

The expected relative error (\mathcal{E}_i) of $c_s(i)$ after two smoothing operations is:

$$\epsilon_i = .24 \frac{1}{\sqrt{k} c_e} \quad (\text{D.1})$$

Since in our experiments $k \approx 14$ runs and $c_e \approx 16.67 = 1000 \times 10 / 600$ (counts/pixel), then,

$$\epsilon_i \approx .065$$

The magnitude of the error of the histogram of distribution of specific ventilation, caused by the statistics of the measuring method, could be estimated analytically by the method described in equation (D.1) or by actually generating a normalized histogram for an "error" image and measuring its spread for each run. The expected error in the specific ventilation histogram for a perfectly homogeneous washout can be calculated by scaling the spread of the error histogram to the number of counts. We chose to use the later method because it included not only the theoretical error but also possible experimental errors from run to run.

The "error" image for run k ($c_{\text{err}}(i,k)$) is defined by dividing the run's equilibration image by the sum of all equilibration images. Assuming that all the equilibration images were proportionally similar, then all pixels of the error image should have values around the number:

$$c_{\text{err}}(i,k) \approx \frac{1}{k}$$

The expected relative error, (σ_i), of an image generated from dividing a given equilibration image by the sum of all of them, after two smoothing operations to both denominator and numerator, is:

$$\sigma(i) \approx \frac{.24}{\sqrt{c_e(i,k)}} \sqrt{1+1/k}$$

which can be estimated for $k=14$ and $c_e \approx 16.7$ counts/pixel as

$$\sigma_i \approx .06.$$

For a totally homogeneous washout, the resulting *MTT* image should be similar to the error image scaled to the total number of counts collected during the washout.

D.3 MTT Correction

The definition OF *MTT* assumes that the measurement is taken from $t=0$ to $t=\infty$. Since the experiments only lasted for a finite time (T) it was necessary to estimate a correction factor in order to account for the difference.

One possible correction could have been to extrapolate to $t=\infty$ the washout curve using the last few points. This, however, could generate large errors because at the end of the washout, the remaining radio-activity level is low and the back-ground noise can be a significant fraction of the signal.

In the following paragraphs the correction algorithm used will be described.

For any washout curve the *MTT* is defined as:

$$MTT = \int_{t=0}^{t=\infty} \frac{c(t)}{c(0)} dt$$

Where $c(0)$ is the initial count rate in (#counts/sec.) and $c(t)$ is the count rate at any time 't'.

Let us call τ the measured value of the integral during the experimental finite time (T).

So,

$$\tau = \int_{t=0}^{t=T} \frac{c(t)}{c(0)} dt = A_1 \quad (D.2)$$

A_1 is defined in figure D-1 as the area under the fractional concentration curve between $t=0$ and $t=T$. A_2 is the error between the measured and the "true" value of the *MTT* estimated from extrapolation.

If we assume now that the washout was mono-exponential with a time constant equal to the actual *MTT*:

$$c(t) = c(0) e^{-(t/MTT)}$$

And solving equation (D.2) yields:

$$A_1 = MTT \{ 1 - e^{-(T/MTT)} \}$$

since $A_1 = \tau$,

$$\tau = MTT \{ 1 - e^{-(T/MTT)} \} \quad (D.3)$$

So, knowing 'T' and τ , the value of the *MTT* can be calculated numerically from equation (D.3). Typical values of *MTT* ranged from 10% for a measured $\tau=90$ sec. to .01% for $\tau=25$ sec. The shaded area in figure D-1 represents the "correction" used in this work and calculated according to equation (D.3)

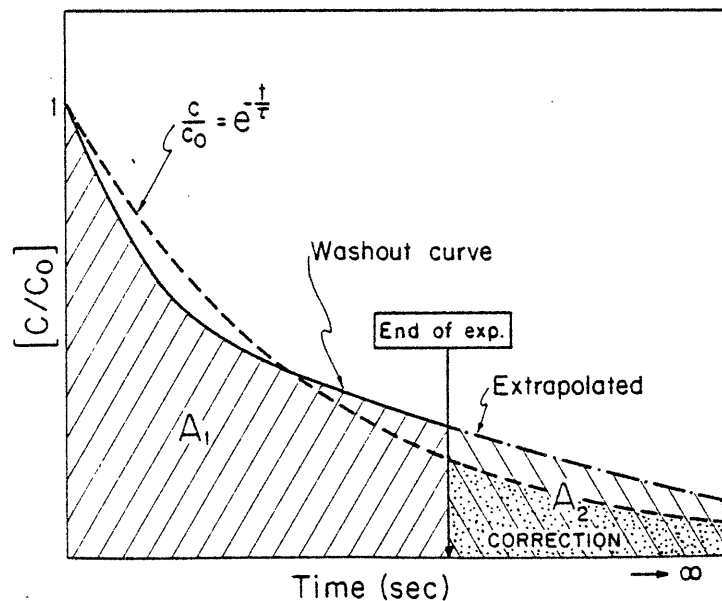


Figure D-1: Plots the fractional concentration of the tracer gas vs time and illustrates graphically the difference between the area calculated using equation (D.3) (shaded), and the correction area that would have been obtained by extrapolating the last points of the curve.

Notice that the error remaining after this manipulation represented by the difference between the "correction area" and A_2 , would be greater for washout curves that depart the most from a single exponential function. Conveniently, the experimental curves with the longest *MTT* were all very close to single exponential functions and the curves with the

shorter *MTT* had a small error since the washout had been almost completed by the time the experiment was finished.

D.4 Relative Error of Volume Measurement

In order to test the hypothesis that the fractional volumes of each region of interest did not change from run to run, the standard deviation of the measured fractional volumes was compared with the expected deviation calculated from the number of counts of each region. The mean and the standard deviation of the measured fractional volumes of the right base and right apex were calculated for dogs 17 to 22. See Table D-I. The relative error was estimated as the ratio of the standard deviation of the measured fractional volumes to the mean (\bar{h}) of the measured fractional volumes. The expected relative error was calculated as the inverse of the square-root of the total number of counts in that region, assuming that there was a total activity $N=1000$ counts per second for a collection period of 10 seconds and that the region was a fraction h of total lung volume.

$$\text{Rel. err.} = \frac{1}{\sqrt{N \times 10 \times h}}$$

A paired T test showed that at a significance level of .05 the observed variation in the measurements of relative lung volumes was equal to the expected variation calculated from the number of counts. Thus, the variations during successive runs of the measured fractional volumes could be explained entirely by the random radioactive decay of the ^{13}NN .

D.5 Histogram Generation

For the histogram generation, the following steps were followed:

1. Generate an image proportional to the uncorrected *MTT* image in the manner described in D.2.

Table D-I:
Comparison between the expected and measured
variations of the regional fractional volume

Region	Mean Fract. Vol	STDEV Fract. Vol.	LUNG VOLUMES.		
			Measured Rel. Err.	Expected Rel. Err.	(<u>Expected</u>) (<u>Measured</u>)
RBA D 22	0.336162	0.003300	0.009817	0.017247	0.569167
RAP D 22	0.172267	0.004922	0.028572	0.024093	1.185880
RBA D 21	0.295329	0.005451	0.018458	0.018401	1.003086
RAP D 21	0.178788	0.004531	0.025342	0.023650	1.071530
RBA D 20	0.356501	0.007562	0.021211	0.016748	1.266467
RAP D 20	0.265133	0.007962	0.030030	0.019421	1.546298
RBA D 19	0.348205	0.007789	0.022368	0.016947	1.319913
RAP D 19	0.153283	0.004290	0.027990	0.025542	1.095829
RBA D 18	0.330441	0.007474	0.022618	0.017396	1.300182
RAP D 18	0.222268	0.004746	0.021352	0.021211	1.006664
RBA D 17	0.338173	0.004823	0.014262	0.017196	0.829378
RAP D 17	0.249113	0.007401	0.029711	0.020036	1.482905
			Mean :	1.139	
			StDev:	0.274	

2. Create a twenty bars Histogram of the previous image. The height of the bar indicates the fraction of lung volume that has an uncorrected *MTT* within a given interval. The intervals are equally spaced each having a width of 5% of the maximum *MTT*.
3. Calculate the uncorrected total *MTT* for the whole lung.
4. Normalize the horizontal scale of the Histogram so that its first moment equals the uncorrected total *MTT* for the lung.
5. Correct the total *MTT* and the horizontal scale of Histogram using equation (D.3) .
6. Calculate the corrected histogram's first moment.
7. Normalize again the horizontal scale so that its first moment equals the corrected value of the whole lung corrected *MTT*.

8. Invert the horizontal scale of 7 to transform it into regional specific ventilation.
(*SPVENT*)
9. Transform the horizontal scale into a fractional deviation from the whole lung
SPVENT. The first moment of the resulting histogram is located at zero.
10. Calculates the Standard deviation of the Histogram from 9.

Appendix E

NON-INVASIVE METHOD TO DIAGNOSE AIRWAY OBSTRUCTION

One difficult medical problem is the early diagnosis of obstruction of a major central airway as may occur in carcinoma of the lung at early stages. This is particularly true when the obstruction is located in one of the first five bronchial generations of the airways and does not dramatically occlude the lumen of the affected bronchus.

An indirect method of detecting airway obstruction is the use of a radioactive tracer gas, such as $^{13}\text{N}_2$ or ^{133}Xe , to image the patients' lungs during a wash-out maneuver at normal spontaneous ventilation. Poorly ventilated regions can be visualized because the mean transit time of the tracer gas in those regions is longer than in healthier zones. This method, however, is very sensitive to parenchymal and small airways disease because the distribution of ventilation during normal breathing is more profoundly influenced by the compliance of the alveolar tissues than by the resistance to airflow of the major airways.

From the results of this study it follows that the distribution of ventilation during *HFV* is more affected by the geometry of the larger airways than during conventional ventilation. This is partially true because, as the tidal volume is decreased, the pressure excursions of the alveolar gas are minimized. A second reason is that, in order to maintain eucapnea, the frequency has to be increased more than proportionally to the decrease of tidal volume. Thus, the mean flow rates in the airways during eucapnic *HFV* exceed the normal flow rates by as much as a factor of ten. Because the larger airways have a relatively small total cross-sectional area, the major pressure drop moves from the alveolar compliance to the larger airways as the ventilatory flow rate increases.

So the basis of the proposed technique is the movement of the primary impedance from

the alveolar compliance to the larger airway resistance¹⁰ If a moderate obstruction exists in one of the major bronchi, breathing at normal respiratory rates will not reveal any significant reduction in flow to the compromised lung volume because any small additional losses associated with the obstruction have a negligible influence on the regional ventilation .

On the strength of the previous discussion, a method for making the presence of the obstructions measurable is to use *HFV* during the wash-out so that the major pressure drop occurs in the bronchial generation that contains the partial obstruction. Then the effects of the obstruction will be amplified and the quantification, by various means of the degree of obstruction, will thereby be facilitated.

By imaging the lungs during the washout maneuver of a radioactive tracer such as ¹³NN it is possible to detect those regions from where the rate of removal of the tracer gas is low. By performing this non-invasive measurement at different ventilatory rates it will be possible to detect not only the bronchus containing the obstruction but also the degree of obstruction from the degree of nonuniformity of washout between well ventilated and poorly-ventilated regions.

Clearly, much knowledge has to be gained before any rational theory for the proposed measurement method can be validated. Optimization of the diagnostic value of the proposed technique will undoubtedly require control of both the ventilation frequency and the tidal volume associated with each breath.

Proposed Confirming Experiments.

Ventilation/perfusion scans are currently being performed at the Mass. General Hospital using the positron camera described in Appendix D.1. Since the standard procedure includes, among other things, a wash-out maneuver at spontaneous respiration, by performing a second

¹⁰This application of *HFV* was first conceived during a conversation that I had with professor Dewey from MIT in October 1982.

wash-out maneuver using *HFV*, the areas ventilated through mildly-obstructed airways will be enhanced.

Medical Significance

The possibility of detecting large bronchial obstructions with a non-invasive method provides an exciting possibility for early tumor detection. A large percentage of lung cancers are initially localized around major airways and are hard to see on Xray because they are lost in other shadows of the hilum. So, those tumors are detected only when the ventilation to the corresponding region of the lung has been dramatically reduced. This method could provide a tool to screen and detect patients with malignant tumors before the disease is too widespread to be treated surgically.

List of Figures

- Figure 2-1:** Schematic of the flow system of the *HFV* ventilator. For detailed description see appendix C 15
- Figure 2-2:** Showing the configuration of inspiratory and expiratory lines and the location of the mean airway pressure catheter. 15
- Figure 2-3:** Graph showing the delivered volume waveform vs time as measured from the pressure oscillations induced by the *HFV* device in a calibration tank. The two charts are for two different settings of V_t and f but the same $(V_t \times f)$ product and the same $E:I=1$. 16
- Figure 2-4:** Schematic showing the experimental apparatus set-up to study the regional distribution of ventilation during *HFV*. 17
- Figure 4-1:** Semi-log scale Plot, of fractional concentration of total ^{13}NN in the lungs vs time for two different washout runs. The settings of V_t and f of the ventilator are included together with the respective visual images collected at 40% of the initial concentration. 25
- Figure 4-2:** The Mean Transit Time images (top), and the corresponding normalized *SPVENT* histograms (bottom), for washout runs from the same animal. For explanation see text. 29
- Figure 4-3:** Graph showing a typical curve of fraction of lung volume vs normalized regional *SPVENT* and its corresponding measurement error estimate. (for explanation see text) 31
- Figure 4-4:** Simple example of the effect of using a two-dimensional image to generate the histograms. For explanation see text. 33
- Figure 4-5:** Showing the histogram and its corresponding two-dimensional image of *MTT* (left), and the histogram that would have been obtained from a hypothetical three-dimensional image of the lung (right). Notice that in the two-dimensional *MTT* image it appears as if the full bases of the lung were hyperventilated, while only a small fraction of such a region could have been hyperventilated. 34
- Figure 5-1:** Experimental results, from dog #18, of whole-lung *SPVENT* plotted vs the product $(V_t \times f)$ for a constant $V_t=80$ (upper curve) and $V_t=40$ cc. (lower curve). Notice the large V_t effect present for the same $(V_t \times f)$. 37
- Figure 5-2:** Experimental results, of whole-lung *SPVENT* vs the product $(V_t \times f)$ from protocol #2. For each of the 6 animals there are two curves; one for a constant $V_t=40$ cc. and another for a constant $V_t=80$ cc. Although the two dotted lines ("g" and "G") are from protocol #1 they are included for comparison with fig. 5-4. 38
- Figure 5-3:** Experimental results for protocol #2 plotted in log-log scales according to the results from dimensional analysis 42
- Figure 5-4:** Same experimental results from figure 5-2 but plotted now according to equation (5.1). 43
- Figure 5-5:** Experimental results from protocol #1 of whole-lung *SPVENT* vs V_t for 7 animals. All the runs were made with constant $(V_t \times f)=400$ cc/sec and $E:I=1$. 44
- Figure 5-6:** Experimental results of whole-lung *SPVENT* vs V_t for constant $(V_t \times f)$ and $E:I=1$ for all dogs of protocol #1. Notice in all cases the linear 45

relation between V_t and $SPVENT$

- Figure 5-7:** Experimental results of whole-lung $SPVENT$ vs V_t for constant $(V_t \times f)$ and $E:I > 1$. There was not a substantial difference between these results and those of figure 5-6 46
- Figure 5-8:** Log-log plot of arterial blood PCO_2 , measured after four minutes of HFV , vs total alveolar ventilation per kg for all dogs of protocol #2. The best fit straight line is also included 48
- Figure 5-9:** Efficiency (η) of HFV and CV plotted vs (V_t/V_d) . For explanations see text 52
- Figure 5-10:** MTT images for dog #16. Each image was obtained from a run with particular settings for V_t and f but all have the same $(V_t \times f) = 400$ cc/sec.. Notice that the larger tidal volumes (images near the top) preferentially ventilated the bases of the lung. 54
- Figure 5-11:** Set of MTT images from protocol #2. The left column contains the ones for the runs made with $V_t = 40$ cc. and the right column the ones for the runs made with $V_t = 80$ cc.. Each row has the same $(V_t \times f)$ product with the higher frequencies located nearer the top. 55
- Figure 5-12:** Experimental results of $SIGMA$ vs V_t for all experiments of protocol #1 with $E:I = 1$. Each curve is made from runs where the product $(V_t \times f)$ was kept constant while V_t was changed. 59
- Figure 5-13:** Experimental results of $(SIGMA)$ vs f for all experiments in protocol #2 with a $V_t = 40$ cc. Each curve corresponds to a different animal 60
- Figure 5-14:** Regional $SPVENT$ vs V_t for a set of three runs from the same dog at a $(V_t \times f) = 300$ cc/sec.. Each curve corresponds to a different region. (RA=right apex, LA=left apex, RB=right base, LB=left base) Notice that the increase in V_t produced a preferential increase in the ventilation of the bases. 61
- Figure 5-15:** Regional $SPVENT$ vs $(V_t \times f)$ for a set of five runs from dog # 21 where V_t was kept constant at 40cc.. Each curve is for each of the four different regions defined in fig(5-14). Notice that in this case, the increase in f produces a more distributed increase in $SPVENT$ among the different compartments than the increase of V_t at constant $(V_t \times f)$. 62
- Figure 5-16:** Experimental results, for all runs in protocol #1 where $E:I = 1$. Here, the ratio of the specific ventilation for the right lung to that to the left lung $RIGHT/LEFT$ is plotted vs V_t . Each curve corresponds to a single animal at a constant $(V_t \times f)$ and $E:I$ 63
- Figure 5-17:** Example of experimental results from dog #20 of protocol #2 where the $RIGHT/LEFT$ ventilation ratio is plotted vs $(V_t \times f)$. For the runs of each curve the V_t was kept constant at 80cc. (triangles) and 40cc. (circles). 64
- Figure 5-18:** Experimental results from all runs in protocol #1 where $E:I = 1$. Here, the ratio of the specific ventilation of the basal regions to that of the apical regions ($BASE/APEX$) is plotted against V_t for constant values of $(V_t \times f)$ 66
- Figure 5-19:** Typical plot of basal over apical specific ventilation vs $(V_t \times f)$ for dog #18, protocol #2 where V_t was kept constant at 40cc. (circles) and at 80cc. (triangles) 67
- Figure 6-1:** Schematic of the central airways illustrating three possible causes of increased flow to the basal regions of the lungs. (For explanation see text) 79
- Figure 6-2:** Simplified electrical analog of the flow distribution between the apex and the base of a lung. For explanation see text 80
- Figure C-1:** Plot of Flow vs time illustrating the way to calculate the tidal volume (V_t) delivered by the HFV device. V_{in} = volume entering the system through the rotary valve. V_{out} = volume leaving the system by the high 101

impedance suction duct.

Figure C-2: Calibration graph for the V_t delivered by the *HFV* device. The 'X' 102
axis is the calculated value of V_t in cubic cm.. The 'Y' axis is the measured
value of V_t from the recorded pressure signal generated on a calibration tank
by the *HFV* device

Figure D-1: Plots the fractional concentration of the tracer gas vs time and 109
illustrates graphically the difference between the area calculated using equation
(D.3) (shaded), and the correction area that would have been obtained by
extrapolating the last points of the curve.

List of Tables

- Table 5-I:** Summary of the statistical analyses for the regional ventilation parameters. For explanation see text 57
- Table 5-II:** Summary of results from partially occluded airway experiments. The numbers on the table are the ratio of the specific ventilation of the unobstructed lobe to that of the obstructed lobe for the cases of balloon-inflated and non-inflated, for both *CV* and *HFV* 69
- Table D-I:** Comparison between the expected and measured variations of the regional fractional volume 111

References

- Akhavan, R. Pressure-flow characteristics of a branching network during oscillatory flow. Master's thesis, MIT, 1982.
- Akhavan, R. (1983). . Personal communication.
- Alpert N.M., McKusick K.A., Correia J.A., Shea W., Brownell G. L., and Postaid M.S. Initial assesment of a simple functional image of ventilation. *Journalofnuclearmedicine*, 1976, 17(2), 88-92.
- Altman L. and D. Pitmer. *Biologic Handbook of Respiration and Circulation*. : Fed. of Am. Soc. for Exp. Biol. 1971.
- Bland R.D., Kim M.H., Light M.J., and Woodson, J.L. High frequency mechanical ventilation in severe hyaline membrane disease. An alternative treatement ? *Crit. Care Med.*, 1980, 8(5), 275-280.
- Boun, D.G.,Miyasaka, K., Marchak, B.E., Thompson, W.K., Froese, A.B., and Bryan, A.C. Ventilation by high frequency oscillation. *JAP*, 1980, 48(4), 710-716.
- Braudi G. Frictional forces at the surface of the lung. *Bull. Physio-path. resp.*, 1972, 8(1), 323-332.
- Brownell G.L. and Burnham C.A. *Recent developments in positron cintigraphy*. : Academic Press 1974.
- Brownell G.L, Correia J.A. Zamenhof R.G. *Recent advances in nuclear medicine volume 3, Chap 1*. : Grune & Stratton, inc 1977.
- Carlson G.C., Ray C. Jr., Peirri M.K., Greogr J., and Howland W.S.: High-frequency jet ventilation. *Chest*, 1982, 81(3), 350-354.
- Chatwin P.C. On the longitudinal dispersion of passive contaminant in oscillatory flows in tubes. *JFM*, 1975, 71(3), 513-527.
- Collins, P.C. Dispersion of a passive contaminant in oscillatory flow within a branching network. Master's thesis, MIT, 1982.
- Fletcher, P.R. and Epstein R.A. Constancy of physiological dead space during high frequency ventilation. *Respiration Physiology*, 1982, 47(1), 39-49.
- Fredberg, J.J. Augmented Diffusion in the airways can support pulmonary gas exchange. *JAP*, 1980, 49(2), 232-238.
- Gavriely, N. and Solway, J. . Personal communication.
- Gavriely , Solway G., Slutsky A., Kamm R., Shapiro A.H., Drazen J. *Effect of endotracheal tube on CO₂ elimination by small volume high frequency ventilation in dogs.* Am Rev of Resp Deceases 125(2)- 232, 1982.

- Haselton F.R. and Scherer P.W. Bronchial bifurcations and respiratory mass transport. *Science*, 1980, 208(1), 69-71.
- Horsfield K., and Cumming, G. Morphology of the bronchial tree in the dog. *Respir. Physiol.*, 1976, 26(), 176-182.
- Joshi C.H., Kamm R.D., Drazen J.M., and Slutsky, A.S. Gas exchange in laminar oscillatory flows. *submitted to the J. Fluid Mech.*, 1982, (), .
- Kamm R.D., Slutsky A.S. and Drazen J.M. High Frequency Ventilation. Submitted for publication in CRC Critical Reviews in Bioengineering.
- Klain, M., and Smith, R. B. High frequency percutaneous jet ventilation. *Crit. Care Med.*, 1977, 5(1), 280-287.
- McEvoy, R.D., N.J.H. Davies, F.L. Mannino, R.J. Prutow, P.T. Scumacker, P.D. Wagner, and J.B. West. Pulmonary gas exchange during high frequency ventilation. *JAP*, 1982, 52(5), 1278-1287.
- Mead J. Mechanical properties of the lung. *Physiological Reviews*, 1961, 41(1), 281-330.
- Paloski W.H., Mullins R.J., Barrie P.S., and Newel J.C. . Nitrogen washout and CO₂ elimination are related during High Frequency ventilation. Am. Fed. of Physiological Soc., March 1982. Published as Vol 41, Number 5, of the federation Proceedings.
- Pizer S. M., Brownell G.L., Chesler D.A. *Instrumentation in nuclear medicine, vol 2, Chap 7.* : Academic press, Inc. 1974.
- Robertson H.T., Coffey R.L., Standaert T.A. and Trog W.E. respiratory and inert gas exchange during high frequency ventilation. *JAP*, 1982, 52(3), 683-689.
- Ross, B.B. Influence of bronchial tree structure on ventilation in dog's lung as inferred from measurements of a plastic cast. *JAP*, 1957, 10(1), 1-14.
- Rossing, T.H., Slutsky, A.S., Lehr, J., Drinker, P., Kamm, R.D., and Drazen, J.M. Tidal volume and frequency dependence of carbon dioxide elimination by high-frequency ventilation. *New England Journal of Medicine.*, 1981, 305(), 1375-1397.
- Scheid P., Kaethner T., Kohl J., and Pipper J. *Gas concentration profiles along the airways of dog lungs during high frequency ventilation.* American Thoracic Society, 1982.
- Schmid, E.R., Knopp, T.J., and Rehder, K. Intrapulmonary gas transport and perfusion during high frequency oscillation. *JAP*, 1981, 51(6), 1507-1514.
- Schuster D.P., Klain M. and Snider J.V. Comparison of high frequency jet ventilation to conventional ventilation during severe acute respiratory failure in humans. *Crit Care Med*, 1982, 10(1), 625.
- Schuster R.C., Snider J.V., Klain M., and Grevic, A. High frequency jet ventilation during the treatment of acute fulminant pulmonary edema. *Chest*, 1981, 80(6), 682-685.
- Secker-Walker R. H., Hill R.I., Markham J., Baker J., Wilhelm J., Alseron O.P., and Potchen

- E. The measurement of regional ventilation in man: a new method of quantitation. *Journal of Nuclear Medicine*, 1973, 14(10), 725-732.
- Sjostrand U. High-frequency Positive-pressure ventilation (HFPPV): a review. *Critical Care Medicine*, 1980, 8(9), 345-364.
- Slutsky, A.S., Drazen, J.M., Ingram, R.H., Kamm, R.D., Shapiro, A.H., Fredberg, J.J., Loring, S.H., and Lehr, J. Effective pulmonary ventilation with small volume oscillations at high frequency. *Science*, 1980, 209(), 609-611.
- Slutsky, A.S., Kamm, R.D., Rossing, T.H., Loring, S.H., Leher, J., Shapiro, A.H., Ingram, R.H., and Drazen, J.M. Effects of frequency, tidal volume and lung volume on CO₂ elimination in dogs by high frequency (2-30 Hz). *J. Clin. Invest.*, 1981, 68(), 1475-1484.
- Snyder B., Dantzker D.R., Jaeger M.J. Flow partitioning in symmetric cascades of branches. *JAP*, 1981, 51(9), 598-606.
- Taylor, G.I. The dispersion of matter in turbulent flow through a pipe. *Proc. R. Soc. Lond. (Biol.)*, 1954, 223(), 446.
- Turbull A.D., Carlon G., Howland W.S., and Batie E.J. High frequency jet ventilation in major airway of pulmonary disruption. *Annals of Thoracic Surgery*, 1980, 32(5), 468-474.
- Venegas José G. Enhancement of flow in collapsible tubes by the application of reversed pressure pulses, with especial reference to chronic obstructive lung disease. Master's thesis, University of Aston in Birmingham (UK), 1975.
- Venegas J.G., Venegas M. Pulsos reversos de presión. Nueva alternativa para el tratamiento de las enfermedades pulmonares obstructivas crónicas. *Tribuna Médica*, 1979, (), 33-42. Reprints can be obtained from (José G. Venegas, Cra 7 #83-36 Apt 302 Bogotá Colombia).
- Venegas J. G. and Venegas M. Reversed Pressure Pulses . English translation of the work awarded the Colombian National Science Prize, 1977. Fundación Alejandro Ángel Escobar, Colombia. Reprints can be obtained from (José G. Venegas, Cra 7 #83-36 Apt 302 Bogotá Colombia).
- Wagner, Saltzman and West. Measurement of continuous distribution of ventilation-perfusion ratios: theory. *JAP*, 1974, 36(1), 88-99.
- Watson, E.J. Diffusion in oscillatory pipe flow. Submitted to *J. Fluid Mech.*
- West J. B. . *Ventilation/Blood Flow and Gas Exchange*. : Oxford:Blackwell 1977.
- West J.B. *Respiratory Physiology -the essentials 2nd Edition*. : Williams & Wilkins 1979.
- Keneth L. Zierler. Equations for measuring blood flow by external monitoring of radioisotopes. *Circulation Research*, 1965, 16(4), 309-321.